applied sciences

MDPI

Article

Operational Modal Analysis for Vibration Control Following Moving Window Locality Preserving Projections for Linear Slow-Time-Varying Structures

Weihua Fu [1], Cheng Wang [1,2,*] and Jianwei Chen [3]

[1] College of Computer Science and Technology, Huaqiao University, Xiamen 361021, China; hqufwh@stu.hqu.edu.cn
[2] Xiamen Engineering Research Centre of Enterprise Interoperability and Business Intelligence, Xiamen 361021, China
[3] Department of Mathematics and Statistics, San Diego State University, San Diego, CA 92182, USA; jianweichen@hqu.edu.cn
* Correspondence: wangcheng@hqu.edu.cn; Tel.: +86-592-6162495

Abstract: Modal parameters can reflect the dynamic characteristics of the structure and can be used to control vibration. To identify the operational modal parameters of linear slow-time-varying structures only from non-stationary vibration response signals, a method based on moving window locality preserving projections (MWLPP) algorithm is proposed. Based on the theory of "time freeze", the method selects a fixed length window and takes the displacement response signal in each window as a stationary random sequence. The locality preserving projections algorithm is used to identify the transient modal frequency and modal shape of the structure at this window. The low-dimensional embedding of the displacement response data set calculated by locality preserving projections (LPP) corresponds to the modal coordinate response matrix, and the transformation matrix corresponds to the modal shape matrix. The simulation results of the mass slow-time-varying three degree of freedom (DOF) and the density slow-time-varying cantilever beam show that the new method can effectively identify the modal shape and modal natural frequency of the linear slow-time-varying only from the non-stationary vibration response signal, and the performance is better than the moving window principal component analysis (MWPCA).

Keywords: operational modal parameters; slow-time-varying structures; non-stationary vibration response signals; moving window; preserving projections algorithm

Citation: Fu, W.; Wang, C.; Chen, J. Operational Modal Analysis for Vibration Control Following Moving Window Locality Preserving Projections for Linear Slow-Time-Varying Structures. *Appl. Sci.* **2021**, *11*, 791. https://doi.org/10.3390/app11020791

Received: 19 November 2020
Accepted: 12 January 2021
Published: 15 January 2021

1. Introduction

Vibration is an inherent property of structures and bad vibrations will cause damage to structures [1]. Operational modal analysis (OMA) identifies structural modal parameters (modal natural frequency, modal shape, damping ratio) from the output displacement response signal of the structure [2,3], which can be used for damage identification [4], structural design [5], structural health monitoring of aircraft wings [6], and building performance assessment [7].

Manifold Learning [8] has become a research focus in information science since it was first proposed in 2000. Assuming that the data are uniformly sampled from a low-dimensional manifold in a high-dimensional Euclidean space, the purpose of manifold learning is to find the low-dimensional embedding in the high-dimensional space and find the corresponding embedded transformation matrix [9]. Based on this concept, the dimensionality reduction process of manifold learning needs to keep the data after dimensionality reduction satisfying the geometric constraint relation related to high-dimensional space manifold. At present, the more widely applied algorithms of manifold learning include principal component analysis (PCA) [10], isometric feature mapping (Isomap) [11], Laplacian eigenmaps (LE) [12], locally linear embedding (LLE) [13] and so on. Many researchers have applied manifold learning to operational modal analysis. Wang et al. used principal component analysis for operational modal parameters identification to solve the problem of false modal in other identification methods [14]. Bai et al. used locally linear embedding to identify operational modal parameters of complex three-dimensional continuous structures [15]. Wang et al. used isometric feature mapping to identify the operational modal parameters of three-dimensional structures [16]. The method mentioned above is suitable for linear time-invariant structures.

However, operational modal parameters of many structures are time-varying [17]. A linear structure whose system parameters (i.e., mass, stiffness, or damping) change over time is called a linear time-varying (LTV) structure. For example, during the flight launch of missile or rocket, the mass of the whole structure is gradually reduced due to the constant consumption of fuel [18]. With the activity of human flow, the structure characteristics of large human gathering places change, such as stadiums [19]. Therefore, time-varying systems are different from constant system. Time-varying structures need to identify time-varying parameters, which can monitor the state of the structures. At present, the time-domain and frequency domain methods are used to identify the operational modal parameters of time-varying structures [20,21]. Zhou et al. analyzed and summarized the advantages and disadvantages of these methods in detail [22]. The time-varying structures can be divided into fast time-varying structures and slow-time-varying structures [23] and Ramnath pointed out the system whose variation in coefficient is much less than variation in solution is called slow time-varying system [24]. For example, when a train passes a bridge quickly, the train works together with the bridge to form a unified dynamic system. The mass distribution and stiffness distribution of the system change rapidly with time, which forms a fast time-varying structural dynamics problem [25]. The mechanical arms in industrial manufacture can be regarded as slow time-varying structures [26]. The vibration response signals of linear slow-time-varying structures cannot be obtained completely at one time, but need to be obtained by continuous sampling over time. Therefore, the moving window method based on the theory of “short time-invariant” can be well applied to the identification of operational modal parameters of linear slow-time-varying structures. At present, the moving window method has been applied to some algorithms to identify the operational modal parameters of linear slow-time-varying structures. Huang et al. proposed moving window EASI algorithm identify the operational modal parameters of the linear slow-time-varying system [27]. Wang et al. proposed a moving window second order blind identification method for identifying operational modal parameters of linear slow-time-varying structures, and the performance of this method is better than the moving window independent component analysis [28]. Guan et al. combined moving window with principal component analysis to effectively identify the operational modal parameters of the slow-time-varying system [29,30]. Huang et al. propose an operational modal analysis (OMA) method that uses eigenvector recursive PCA with a forgetting factor to identify the transient natural frequencies and transient modal shapes [31].

In addition, there are many time-domain methods for operational modal analysis. Some methods involve choosing a mathematical model to idealize the structural dynamic responses, including autoregressive moving average (ARMA) [32] and autoregressive (AR) model updating [33]. Based on singular value decomposition and QR factorization, Barros-Rodriguez et al. proposed a new method and applied it to the analysis of F-18 flutter flight test data. The method is capable of identifying the frequency and damping of the critical aircraft modes, those responsible for the flutter phenomenon [34]. Chen et al. developed a novel method for moving force identification (MFI) called preconditioned least square QR factorization (PLSQR) method which seeks to reduce the impact of identification errors caused by unknown noise [35]. Some methods, such as time–frequency analysis method, can use the response signal of a vibration sensor to identify multi-modal parameters, but generally can only identify the natural frequency and damping ratio of multi-modal, but cannot identify modal shapes.

Locality preserving projections (LPP) is a linear dimensionality reduction method [36], which makes it fast and suitable for practical application. In addition, LPP has several nonlinear technology data representation characteristics, which makes it more accurate in preserving data characteristics. Therefore, a method based on moving window locality preserving projections (MWLPP) is proposed to identify the operational modal parameters of linear slow-time-varying structures. LPP first calculates the transformation matrix of mapping the high-dimensional data to the low-dimensional space, and then computes the low-dimensional embedding. The primary contributions of the article can be summarized as follows:

(1) An operational modal parameter identification method based on LPP is proposed. The main idea is to find out the one-to-one correspondence between the coordinate response matrix and the low-dimensional embedded data, and the one-to-one correspondence between the modal shape matrix and the transformation matrix. The operational modal parameter identification problem can be transformed into the manifold dimension reduction problem of structural vibration response data.
(2) The LPP algorithm and moving window method are combined to identify the operational modal parameters of linear slow-time-varying structures.
(3) By comparing the operational modal parameter identification method based on moving window principal component analysis method, MWLPP has higher accuracy and effectively reduces the modal missing.
(4) To verify the identification ability of operational modal parameters of linear slow time-varying structures based on MWLPP, a mass slow-time-varying 3-DOF (degree of freedom) structure and a density slow-time-varying cantilever beam structure were designed. The MWPCA method was used to identify the operational modal parameters of non-stationary vibration response simulation data for comparison.

The remainder of this paper is organized as follows. In Section 2, The LPP algorithm is introduced to identify the operational modal parameters of linear time-invariant structures. The moving window combined with LPP algorithm is introduced to identify the operational modal parameters of linear slow-time-varying structures in Section 3. Section 4 presents the simulation verification results. Finally, we make a conclusion in Section 5.

2. OMA of Linear Time-Invariant Structures Based on LPP

2.1. Problem of OMA of Linear Time-Invariant Structures

According to the dynamic theory of the structure, the dynamic equation of n degrees of freedom (DOF) linear time-invariant vibration structure in the physical coordinate system is:

$$\mathbf{M}\ddot{\mathbf{X}}(t) + \mathbf{C}\dot{\mathbf{X}}(t) + \mathbf{K}\mathbf{X}(t) = \mathbf{F}(t) \tag{1}$$

where $\mathbf{M} \in \mathbb{R}^{n\times n}$, $\mathbf{C} \in \mathbb{R}^{n\times n}$ and $\mathbf{K} \in \mathbb{R}^{n\times n}$ are the mass matrix, damping matrix, and stiffness matrix of the structure. T is number of sampled data points. $\mathbf{X}(t) \in \mathbb{R}^{n\times T}$, $\dot{\mathbf{X}}(t) \in \mathbb{R}^{n\times T}$ and $\ddot{\mathbf{X}}(t) \in \mathbb{R}^{n\times T}$ are the time-domain sampling matrix of the displacement response signal, velocity response signal and acceleration response signal of the structure. $\mathbf{F}(t) \in \mathbb{R}^{n\times T}$ is the time-domain sampling matrix of the external excitation.

The displacement response signal $\mathbf{X}(t) = [\vec{x}_1(t), \vec{x}_2(t), \cdots, \vec{x}_n(t)]^T \in \mathbb{R}^{n\times T}$ of n DOF small damping structure in modal coordinates is:

$$\mathbf{X}(t) \approx \mathbf{\Phi}\mathbf{Q}(t) = \sum_{i=1}^{d} \vec{\phi}_i \vec{q}_i(t) \tag{2}$$

where d is modal truncation and ranges from 1 to n. $\mathbf{\Phi} = [\vec{\phi}_1, \vec{\phi}_2, \cdots, \vec{\phi}_i, \cdots, \vec{\phi}_d] \in \mathbb{R}^{n\times d}$ is the modal shape matrix constituted by d order modal shape $\vec{\phi}_i \in \mathbb{R}^{n\times 1} (i = 1, 2, \cdots, d)$. $\mathbf{Q}(t) = [\vec{q}_1(t), \vec{q}_2(t), \cdots, \vec{q}_i(t), \cdots \vec{q}_d(t)]^T \in \mathbb{R}^{d\times T}$ is a modal response matrix constituted by d order modal response $\vec{q}_i(t) \in \mathbb{R}^{1\times T}(i = 1,2,\cdots,d)$. The main idea of OMA is to identify the modal shape matrix $\mathbf{\Phi} \in \mathbb{R}^{n\times d}$ and modal response matrix $\mathbf{Q}(t) \in \mathbb{R}^{d\times T}$ of the structure only from the vibration displacement response signal $\mathbf{X}(t) \in \mathbb{R}^{n\times T}$. Finally, the natural frequency f and damping ratio ξ are identified by using the single degree of freedom (DOF) technique [37] from the modal response matrix $\mathbf{Q}(t) \in \mathbb{R}^{d\times T}$. For example, the natural frequency f was identified by fast Fourier transform (FFT), and the damping ratio ξ was identified by the random decrement technique (RDT) and the Hilbert transform (HT) from the modal response matrix $\mathbf{Q}(t) \in \mathbb{R}^{d\times T}$. The idea was proposed in [38,39]. When the value of each natural frequency is different, The main modal shape $\vec{\phi}_i$ satisfies normalized orthogonality and the modal response $\vec{q}_i(t)$ of each other is independent.

$$\mathbf{\Phi}^T\mathbf{\Phi} = \mathbf{I}_{d\times d} \tag{3}$$

$$\mathbf{Q}(t)(\mathbf{Q}(t))^T = \mathbf{\Lambda}_{d\times d} = \begin{bmatrix} \vec{q}_1(t)(\vec{q}_1(t))^T & \cdots & 0 & \cdots & 0 \\ \vdots & \ddots & \vdots & \ddots & \vdots \\ 0 & \cdots & \vec{q}_i(t)(\vec{q}_i(t))^T & \cdots & 0 \\ \vdots & \ddots & \vdots & \ddots & \vdots \\ 0 & \cdots & 0 & \cdots & \vec{q}_d(t)(\vec{q}_d(t))^T \end{bmatrix} = \begin{bmatrix} \boldsymbol{\alpha}_k & \cdots & 0 & \cdots & 0 \\ \vdots & \ddots & \vdots & \ddots & \vdots \\ 0 & \cdots & \boldsymbol{\alpha}_i & \cdots & 0 \\ \vdots & \ddots & \vdots & \ddots & \vdots \\ 0 & \cdots & 0 & \cdots & \boldsymbol{\alpha}_d \end{bmatrix} \tag{4}$$

2.2. OMA of Linear Time-Invariant Structures Based on LPP

LPP is a dimensionality reduction algorithm that preserves the geometric relations within the data set. A dataset of T real valued vectors $\mathbf{X}(t) = \{\vec{x}_1(t), \vec{x}_2(t), \cdots \vec{x}_k(t) \cdots, \vec{x}_n(t)\}^T \in \mathbb{R}^{n\times T}$, $\vec{x}_k(t) \in \mathbb{R}^{1\times T}$ in $\mathbb{R}^{n\times n}$ space is located on a smooth d-dimensional manifold ($d \ll n$). LPP calculates the low-dimensional embedding $\mathbf{S}(t) = \{\vec{s}_1(t), \vec{s}_2(t), \cdots \vec{s}_k(t) \cdots, \vec{s}_d(t)\}^T \in \mathbb{R}^{d\times T}$, $\vec{s}_k(t) \in \mathbb{R}^{1\times T}$ in $\mathbb{R}^{d\times d}$ space, which has the same geometric properties as $\mathbf{X}(t)$. There is a transformation matrix $\mathbf{A}$ that makes $\vec{s}_i(t) = \mathbf{A}^T\vec{x}_i(t)$, $x_{ij} \in \vec{x}_i(t) \in \mathbb{R}^{n\times 1}, 1 \le i \le T, 1 \le j \le n$, $\vec{s}_i(t) \in \mathbb{R}^{d\times 1}$. LPP calculates the d-dimensional embedding process of n-dimensional data as follows.

(1) Construct an adjacent-graph G of T real valued vectors in $\mathbb{R}^{n\times n}$ space: K nearest neighbor points of the node $\vec{x}_i(t)(i = 1,2,\cdots i\cdots j\cdots,T)$ are obtained by using the K-neighbor algorithm. If $\vec{x}_j(t)$ is in the K nearest neighbor of $\vec{x}_i(t)$, a directed edge $(\vec{x}_i(t), \vec{x}_j(t))$ is placed.
(2) Calculate the weight of the edge: let the matrix $\mathbf{W} \in \mathbb{R}^{T\times T}$ represents the weight matrix, and w_{ij} is the weight of the edge $(\vec{x}_i(t), \vec{x}_j(t))$. The weights of the connected edges are calculated by heat kernel $w_{ij} = e^{-\frac{\|\vec{x}_i(t)-\vec{x}_j(t)\|^2}{\sigma}}$. If the two nodes are not connected, the weight is 0.
(3) Calculate transformation matrix $\mathbf{A}$: the eigenvectors and eigenvalues of the generalized eigenvector problem are calculated as follows.

$$\mathbf{X}(t)\mathbf{L}\mathbf{X}^T(t)\vec{a} = \lambda\mathbf{X}(t)\mathbf{D}\mathbf{X}^T(t)\vec{a} \tag{5}$$

where the diagonal matrix $\mathbf{D} \in \mathbb{R}^{T\times T}(D_{ii} = \sum_j w_{ji})$ is the degree matrix of graph G, $\mathbf{L} = \mathbf{D} - \mathbf{W}$ is the Laplacian matrix.
(4) Let the column vector set $\left\{\vec{a}_0, \vec{a}_1, \cdots, \vec{a}_{d-1}\right\}$ correspond to the eigenvector of Equation (5) to be solved, order according to their eigenvalues $\lambda_0 \le \lambda_1 \le \cdots \le \lambda_{d-1}$, The low-dimensional embedded vector $\vec{s}_i(t)$ of $\vec{x}_i(t)$ is represented as follows.

$$\vec{s}_i(t) = \mathbf{A}^T\vec{x}_i(t) \tag{6}$$

$$\mathbf{A} = \left\{ \vec{a}_0, \vec{a}_1, \cdots, \vec{a}_{d-1} \right\} \in \mathbb{R}^{n \times d} \tag{7}$$

where Vector $\vec{a}_i(i = 1, 2, \cdots, d-1)$ satisfies normalized orthogonality.

$$\mathbf{A}^T\mathbf{A} = \mathbf{I}_{d \times d} \tag{8}$$

Then, $\mathbf{X}(t) = \left\{ \vec{x}_1(t), \vec{x}_2(t), \cdots \vec{x}_k(t) \cdots, \vec{x}_n(t) \right\}^T \in \mathbb{R}^{n \times T}$ can be decomposed as follows.

$$\mathbf{X}(t) = (\mathbf{A}\mathbf{A}^T)\mathbf{X}(t) = \mathbf{A}(\mathbf{A}^T\mathbf{X}(t)) \tag{9}$$

where $\mathbf{A} \in \mathbb{R}^{n \times d}$ is the transformation matrix, $\mathbf{A}^T\mathbf{X}(t)$ is the d-dimensional embedding $\mathbf{S}(t) \in \mathbb{R}^{d \times T}$ of $\mathbf{X}(t) \in \mathbb{R}^{n \times T}$. Therefore, $\mathbf{X}(t) \in \mathbb{R}^{n \times T}$ has the following form:

$$\mathbf{X}(t) = \mathbf{A}\mathbf{S}(t) = \sum_{i=1}^{d} \vec{a}_i \vec{s}_i(t) \tag{10}$$

Comparing Equations (2) and (10), we can make the conclusion that the low-dimensional embedded $\mathbf{S}(t) \in \mathbb{R}^{d \times T}$ corresponds to the modal response $\mathbf{Q}(t) \in \mathbb{R}^{d \times T}$, and the transformation matrix $\mathbf{A} \in \mathbb{R}^{n \times d}$ corresponds to the modal shape $\mathbf{\Phi} \in \mathbb{R}^{n \times d}$. Figure 1 illustrates OMA of time-invariant structure based on LPP algorithm.

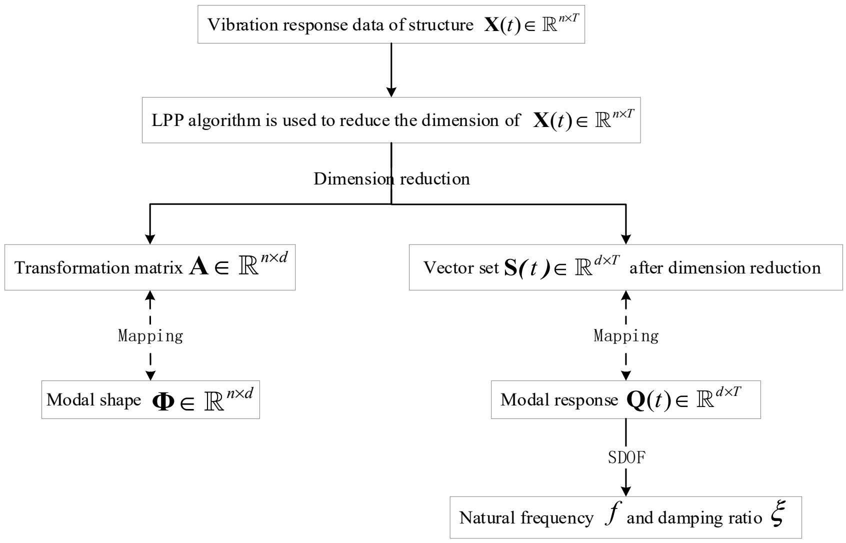

Figure 1. Operational modal analysis (OMA) of time-invariant structure based on locality preserving projections (LPP) algorithm.

Compared with State matrix eigen-decomposition, LPP algorithm builds a graph incorporating neighborhood information of the data set. Using the notion of the Laplacian of the graph, LPP algorithm computes a transformation matrix which maps the data points to a subspace. This linear transformation optimally preserves local neighborhood information in a certain sense [36]. This feature helps retain information about the response signal.

3. OMA of Linear Time-Varying Structure Based on MWLPP

3.1. Problem of OMA of Linear Time-Varying Structure

The operational modal parameters of time-varying structures vary with time. According to the dynamic theory of the structure, the motion equation of a linear time-varying structure of n degrees of freedom in the physical coordinate system in $t \in [T_{BEGIN}, T_{END}]$ is,

$$N : \mathbf{M}(t)\ddot{\mathbf{X}}(t) + \mathbf{C}(t)\dot{\mathbf{X}}(t) + \mathbf{K}(t)\mathbf{X}(t) = \mathbf{F}(t),\ t \in [T_{BEGIN}, T_{END}] \tag{11}$$

where $\mathbf{M}(t) \in \mathbb{R}^{n\times n}$, $\mathbf{C}(t) \in \mathbb{R}^{n\times n}$ and $\mathbf{K}(t) \in \mathbb{R}^{n\times n}$ are the mass matrix, damping matrix, and stiffness matrix of the time-varying structure. $\mathbf{X}(t) \in \mathbb{R}^{n\times T}$, $\dot{\mathbf{X}}(t) \in \mathbb{R}^{n\times T}$ and $\ddot{\mathbf{X}}(t) \in \mathbb{R}^{n\times T}$ are the time-domain sampling matrix of the displacement response signal, velocity response signal and acceleration response signal of the time-varying structure. $\mathbf{F}(t) \in \mathbb{R}^{n\times T}$ is the time-domain sampling matrix of the external excitation.

According to the "time-freezing" theory [40], the mass, damping ratio and stiffness of a linear time-varying structure can be regarded as time-invariant for a short time $\tau \in [t_{begin}, t_{end}]$. Therefore, Equation (11) can be expressed as a set N' consisting of a finite number of linear time-invariant structures $N'(\tau)(\tau \in [t_{begin}, t_{end}])$ within the complete time $t \in [T_{BEGIN}, T_{END}]$.

$$\begin{cases} N' \triangleq \left\{N'(\tau) : \mathbf{M}(\tau)\ddot{\mathbf{X}}(\tau) + \mathbf{M}(\tau)\dot{\mathbf{X}}(\tau) + \mathbf{M}(\tau)\mathbf{X}(\tau) = \mathbf{F}(\tau), (\tau \in [t_{begin}, t_{end}] \subset (t \in [T_{BEGIN}, T_{END}])\right\} \\ \tau = \frac{1}{2}(t_{begin} + t_{end}) = \frac{1}{2}(t_k + t_{k+1}), k = 0, 1, \cdots, K \\ t_0 = T_{BEGIN}, t_K = T_{END} \end{cases} \tag{12}$$

The vibration response data of linear time-varying structures can be divided into a finite number of time-invariant parts by selecting moving window with fixed length L ($\tau \in [t_{begin}, t_{end}]$). The displacement response signal $\mathbf{X}_L^i(\tau) \in \mathbb{R}^{n\times L}$ in the i-th ($\tau \in [t_{begin}, t_{end}]$) window is decomposed into the following Equation (13) in modal coordinates.

$$\mathbf{X}_L^i(\tau) \approx \mathbf{\Phi}_L^i \mathbf{Q}_L^i(\tau) = \sum_{j=1}^{d} \vec{\phi}_j^{\,i} \vec{q}_j^{\,i}(\tau) \tag{13}$$

where $\mathbf{\Phi}_L^i = [\vec{\phi}_1^{\,i}, \vec{\phi}_2^{\,i}, \cdots, \vec{\phi}_d^{\,i}] \in \mathbb{R}^{n\times d}$ is the modal shape matrix formed by the modal shape vector $\vec{\phi}_j^{\,i}(j = 1, 2, \cdots, d) \in \mathbb{R}^{n\times 1}$ of the structure in the i-th ($\tau \in \left[t_{begin}, t_{end}\right]$) window. $\mathbf{Q}_L^i(t) = [\vec{q}_1^{\,i}(t), \vec{q}_2^{\,i}(t), \cdots, \vec{q}_d^{\,i}(t)]^T \in \mathbb{R}^{d\times L}$ is the modal response matrix formed by the modal response vector $\vec{q}_j^{\,i}(t) \in \mathbb{R}^{1\times L}(j = 1, 2, \cdots, d)$ of the structure in i-th ($\tau \in \left[t_{begin}, t_{end}\right]$) window. When the order of each natural frequency is different, The main modal shape $\vec{\phi}_j^{\,i}$ satisfies normalized orthogonality and the modal response $\vec{q}_j^{\,i}$ of each other is independent.

$$(\mathbf{\Phi}_L^i)^T \mathbf{\Phi}_L^i = \mathbf{I}_{d\times d} \tag{14}$$

$$\mathbf{Q}_L^i(t)(\mathbf{Q}_L^i(t))^T = \mathbf{\Lambda}_{d\times d}^i = \begin{bmatrix} \vec{q}_1^{\,i}(t)(\vec{q}_1^{\,i}(t))^T & \cdots & 0 & \cdots & 0 \\ \vdots & \ddots & \vdots & \ddots & \vdots \\ 0 & \cdots & \vec{q}_{k'}^{\,i}(t)(\vec{q}_{k'}^{\,i}(t))^T & \cdots & 0 \\ \vdots & \ddots & \vdots & \ddots & \vdots \\ 0 & \cdots & 0 & \cdots & \vec{q}_d^{\,i}(t)(\vec{q}_d^{\,i}(t))^T \end{bmatrix} = \begin{bmatrix} \alpha_1^i & \cdots & 0 & \cdots & 0 \\ \vdots & \ddots & \vdots & \ddots & \vdots \\ 0 & \cdots & \alpha_{k'}^i & \cdots & 0 \\ \vdots & \ddots & \vdots & \ddots & \vdots \\ 0 & \cdots & 0 & \cdots & \alpha_d^i \end{bmatrix} \tag{15}$$

3.2. OMA of Linear Time-Varying Structure Based on MWLPP

Based on the "time freeze theory" and fixed window length moving windows (MW), the non-stationary signals in each window are regarded as stationary signals. The vibration response signals in the window are identified by using the linear time-invariant OMA method. After OMA of the window is completed, the window moves to the right to delete some old data and add new data to form the vibration response data of the next window. A window corresponds to a moment, so as to identify the operational modal parameters of that moment. Finally, the modal parameter identification results of all windows (moments) are connected to form a continuous result. Moving windows has fixed window length L and moving step λ. Figure 2 shows the process of moving the moving window.

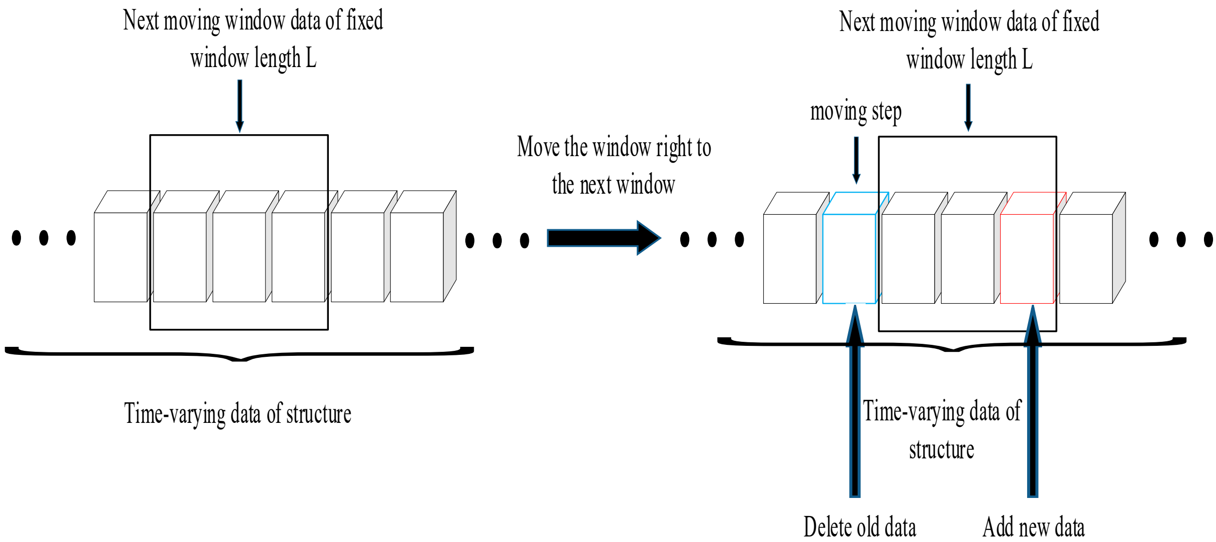

Figure 2. The process of moving the moving window.

Therefore, moving windows are used to track the time-varying properties of the structure. Comparing Equations (2) and (13), it can be seen that the decomposition of vibration response signals in the fixed window length window is consistent with the decomposition of vibration response signals in the linear time-invariant structure. The low-dimensional embedded $\mathbf{S}_L^i(\tau) \in \mathbb{R}^{d\times L}$ of $\mathbf{X}_L^i(\tau) \in \mathbb{R}^{n\times L}$ corresponds to the modal response $\mathbf{Q}_L^i(\tau) \in \mathbb{R}^{d\times L}$, and the transformation matrix $\mathbf{A}_L^i \in \mathbb{R}^{n\times d}$ corresponds to the modal shape $\mathbf{\Phi}_L^i \in \mathbb{R}^{n\times d}$. Suppose the data set is $\mathbf{X}(t) \in \mathbb{R}^{n\times T}$, Figure 3 illustrates the moving window principle processing with time. Figure 4 illustrates OMA of linear time-varying structure based on MWLPP algorithm.

$$\mathbf{X}(t) = \begin{bmatrix} \vec{x}_1(t) \\ \vec{x}_2(t) \\ \vdots \\ \vec{x}_j(t) \\ \vdots \\ \vec{x}_n(t) \end{bmatrix} = \begin{bmatrix} x_1(1) & x_1(2) & \cdots & x_1(i) & x_1(\mathrm{i}+1) & \cdots & x_1(i+L-1) & x_1(\mathrm{i}+L) & \cdots & x_1(\mathrm{T}-1) & x_1(\mathrm{T}) \\ x_2(1) & x_2(2) & \cdots & x_2(i) & x_2(\mathrm{i}+1) & \cdots & x_2(i+L-1) & x_2(\mathrm{i}+L) & \cdots & x_2(\mathrm{T}-1) & x_2(\mathrm{T}) \\ \vdots & \vdots & \ddots & \vdots & \vdots & \ddots & \vdots & \vdots & \ddots & \vdots & \vdots \\ x_\mathrm{j}(1) & x_\mathrm{j}(2) & \cdots & x_\mathrm{j}(i) & x_\mathrm{j}(\mathrm{i}+1) & \cdots & x_\mathrm{j}(i+L-1) & x_\mathrm{j}(\mathrm{i}+L) & \cdots & x_\mathrm{j}(\mathrm{T}-1) & x_\mathrm{j}(\mathrm{T}) \\ \vdots & \vdots & \ddots & \vdots & \vdots & \ddots & \vdots & \vdots & \ddots & \vdots & \vdots \\ x_n(1) & x_n(2) & \cdots & x_n(i) & x_n(\mathrm{i}+1) & \cdots & x_n(i+L-1) & x_n(\mathrm{i}+L) & \cdots & x_n(\mathrm{T}-1) & x_n(\mathrm{T}) \end{bmatrix} \in \mathbb{R}^{n\times \mathrm{T}}$$

$$\mathbf{X}_L^{(1)}(\tau) \longrightarrow \mathbf{X}_L^{(\mathrm{i})}(\tau) \longrightarrow \mathbf{X}_L^{(\mathrm{T-L+1})}(\tau)$$

Figure 3. The moving window principle processing with time.

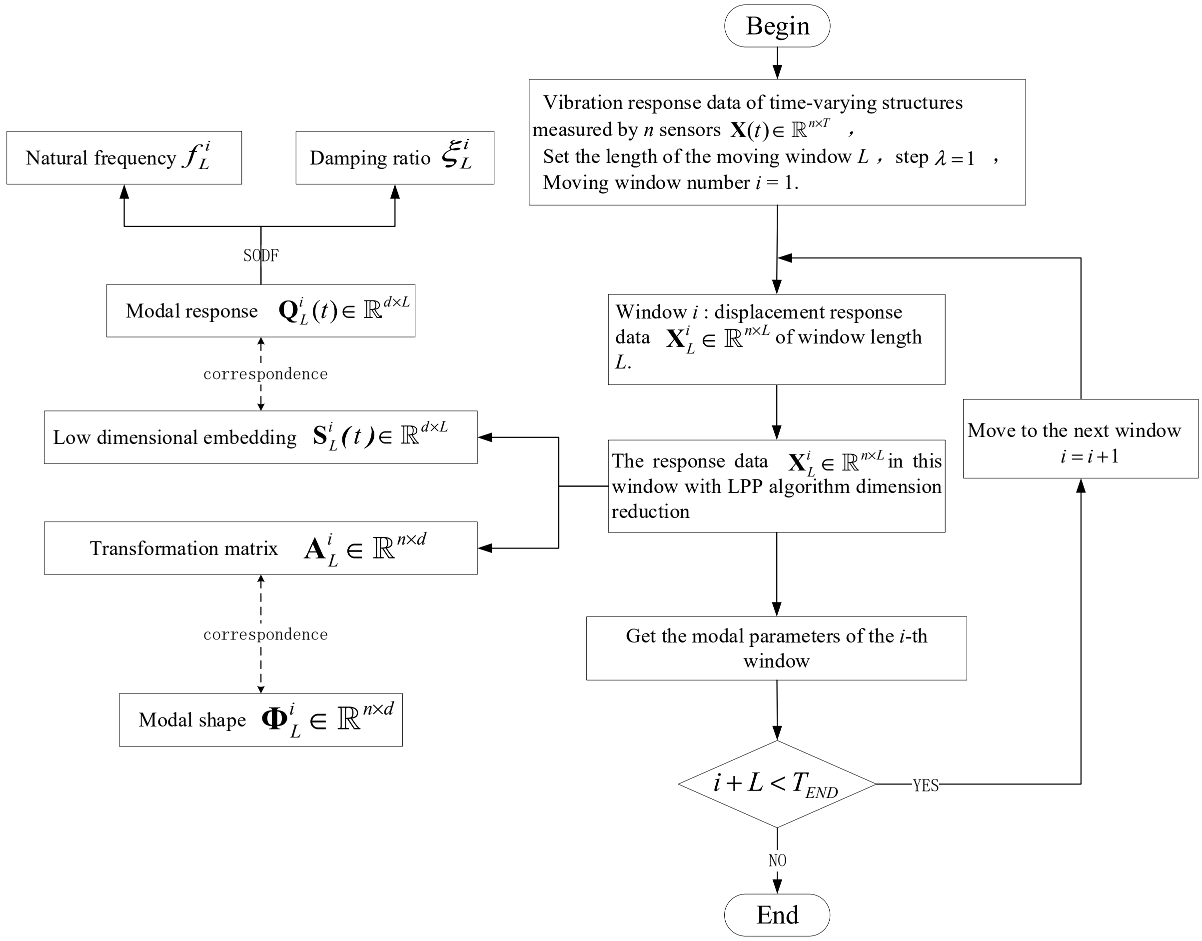

Figure 4. OMA of linear time-varying structure based on moving window locality preserving projections (MWLPP) algorithm.

3.3. The Applicable Scope of the Method

In this paper, the application scope of MWLPP for OMA of linear slow-time-varying structure is,

(1) The method is only suitable for linear slow-time-varying structures with small damping. If the damping is too high, the modals will be complex. Reference [16] show that the damping ratio reaches 10%, and the operational modal parameters can also be identified by manifold learning. However, the lower the damping ratio, the better the identification of modal parameters effect. Only for linear slow-time-varying structures, based on the "time-freezing" theory, Equation (12) can be expressed as Equation (13).

(2) The number of vibration response sensors n should be greater than or equal to the d-order modal identified by the method. According to Equation (2), the displacement response signal in modal coordinates is approximately represented by d-order modal ($d \leq n$). In addition, MWLPP can identify modal natural frequency, modal shape, and damping ratio of one mode with only 1 sensor.

(3) The excitation vector to the structure should be approximately stationary Gaussian white noise.

(4) The method can identify time-varying transient modal shapes, modal frequencies, and modal damping ratios from non-stationary vibration response signals. However, for linear slow-time-varying structures, mass reduction or motion will generate additional damping [41,42]. Therefore, the damping ratio identified by MWLPP cannot be directly compared with real values.

4. Simulation Verification

To verify the identification ability of operational modal parameters of linear slow time-varying structures based on MWLPP, a mass slow-time-varying 3-DOF structure and a density slow-time-varying cantilever beam structure were designed. The moving window principal component analysis (MWPCA) method was used to identify the operational modal parameters of non-stationary vibration response simulation data for comparison.

4.1. An Introduction to Simulation Systems and Data Sets

A mass slow-time-varying 3-DOF structure and a density slow-time-varying cantilever beam are designed in Matlab/Simulink. More simulation details are available in [28,30]. In the simulation, all the natural frequencies in finite element analysis (FEA) are real natural frequency, and the modal shapes in FEA are real modal shapes. In addition, 10% white Gaussian noise is added to the vibration displacement response signal of the slow-time-varying 3-DOF structure, and the modal parameters of the structure are identified.

4.1.1. A Mass Slow-Time-Varying 3-DOF Structure

The mass slow-time-varying 3-DOF structure is designed in Matlab/Simulink. The model of the structure is shown in Figure 5. The dynamic equation of the structure is shown in Equation (16).

$$\begin{bmatrix} m_1(t) & 0 & 0 \\ 0 & m_2(t) & 0 \\ 0 & 0 & m_3(t) \end{bmatrix}\begin{bmatrix} \ddot{x}_1(t) \\ \ddot{x}_2(t) \\ \ddot{x}_3(t) \end{bmatrix} + \begin{bmatrix} c_1+c_2 & -c_2 & 0 \\ -c_2 & c_2+c_3 & -c_3 \\ 0 & -c_3 & c_3 \end{bmatrix}\begin{bmatrix} \dot{x}_1(t) \\ \dot{x}_2(t) \\ \dot{x}_3(t) \end{bmatrix} + \begin{bmatrix} k_1+k_2 & -k_2 & 0 \\ -k_2 & k_2+k_3 & -k_3 \\ 0 & -k_3 & k_3 \end{bmatrix}\begin{bmatrix} x_1(t) \\ x_2(t) \\ x_3(t) \end{bmatrix} = \begin{bmatrix} F_1(t) \\ 0 \\ 0 \end{bmatrix} \quad (16)$$

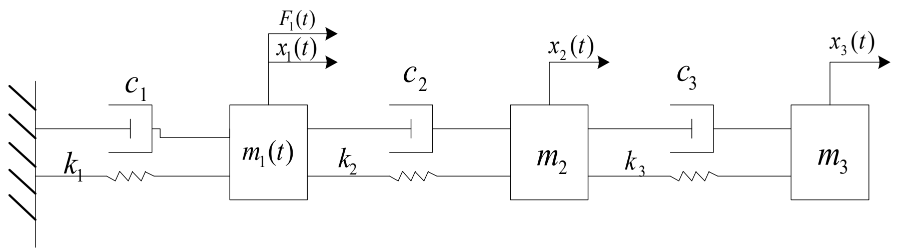

Figure 5. The mass slow-time-varying 3-DOF (degree of freedom) structure with external force.

The structural parameters are as follows: The damping ratio of the three objects is $c_1 = c_2 = c_3 = 0.01(\mathrm{Ns/m})$; the stiffness is $k_1 = k_2 = k_3 = 1000(\mathrm{N/m})$; the initial displacement is 0. The quality is $m_2 = m_3 = 1\mathrm{kg}$. The mass m_1 are time-varying, and the change rule is shown in the following Equation (17).

$$m_1(t) = \begin{cases} 1,\ t \le 50\,\mathrm{s} \\ e^{-0.0005(t-50)},\ 50\,\mathrm{s} < t \le 2000\,\mathrm{s} \end{cases} \quad (17)$$

$F_1(t)$ is white Gaussian noise, and is applied to object m_1. The simulation consists of two parts. In $t \le 50\,\mathrm{s}$, the mass of object m_1 is constant value. In $50\,\mathrm{s} < t \le 2000\,\mathrm{s}$, the mass of object m_1 changes with time, and the system becomes a linear time-varying structure. The 3-DOF simulation structure has only third order mode at most. From Table 1, the highest natural frequency of the third order mode is relatively small, much less than 20 Hz. In general, the higher the sampling frequency is set, the more accurate the modal parameter identification results will be. However, at the same time, the vibration response semaphore and calculation amount of sampling will also be larger. Therefore, according to Nyquist theorem, the sampling frequency is set to 40 Hz, and the sampling interval of simulation is 0.025 s. The displacement response signal data set $\mathbf{X}(t) \in \mathbb{R}^{n\times T}$ of the structure is obtained by Runge-Kutta algorithm in Matlab/Simulink module. The data set $\mathbf{X}(t) \in \mathbb{R}^{n\times T}$ of three degrees of freedom structure is shown in Figure 6, and the sampling duration is 2000 s. Therefore, the final data set is $\mathbf{X}(t) \in \mathbb{R}^{3*80{,}000}$.

Table 1. The real natural frequency of the mass slow-time-varying 3-DOF structure when t = 50.025 s, t = 1200 s and t = 1974.375 s.

	Real Natural Frequency (Hz)		
Order	**t = 50.025 s**	**t = 1200 s**	**t = 1974.375 s**
1	2.24	2.29	2.31
2	6.28	7.02	7.27
3	9.07	10.56	12.26

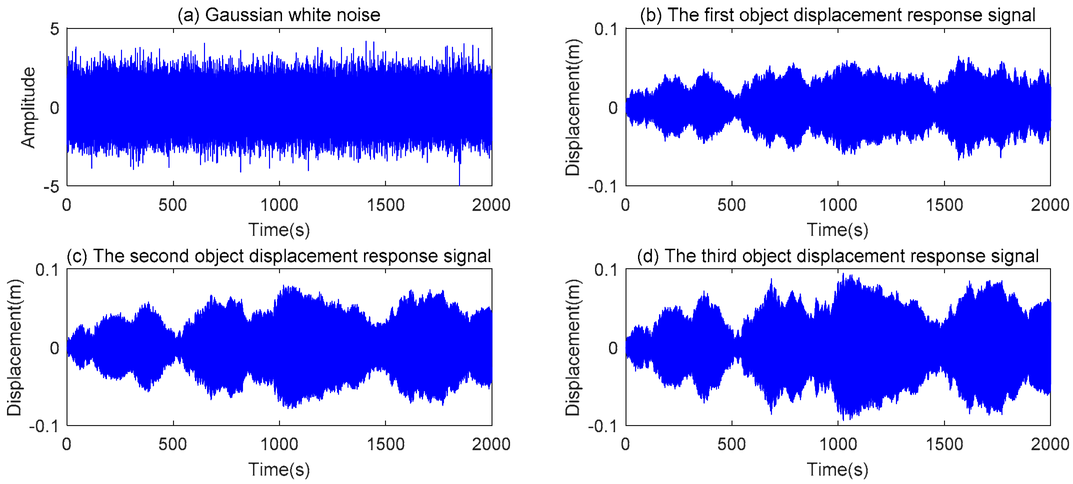

Figure 6. The Gaussian white noise and three object displacement response signal graphs. (**a**) Gaussian white noise; (**b**) The first object displacement response signal; (**c**) The second object displacement response signal; (**d**) The third object displacement response signal.

The real natural frequency of the structure is shown in Figure 7. The real natural frequencies at t = 50.025 s, t = 1200 s and t = 1974.375 s are shown in Table 1 below. The natural frequencies identified by MWLPP at t = 50.025 s, t = 1200 s and t = 1974.375 s are shown in Figure 8.

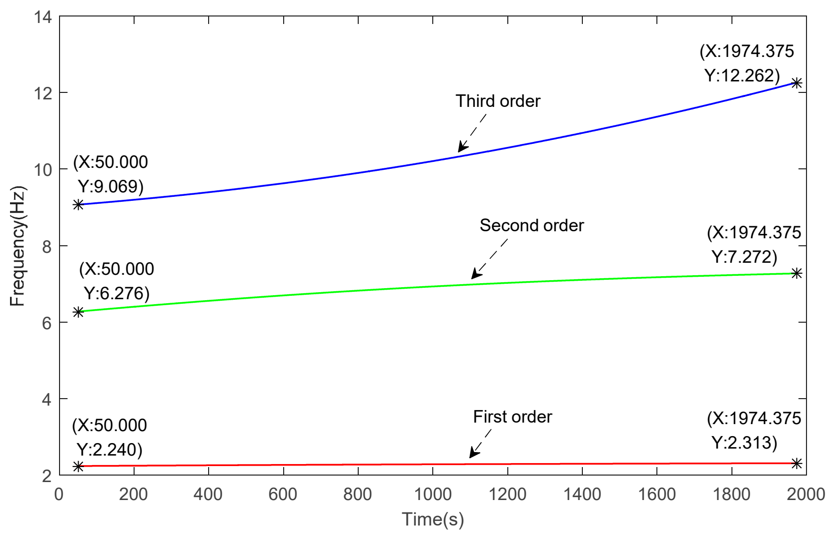

Figure 7. The real natural frequency of the mass slow-time-varying 3-DOF structure.

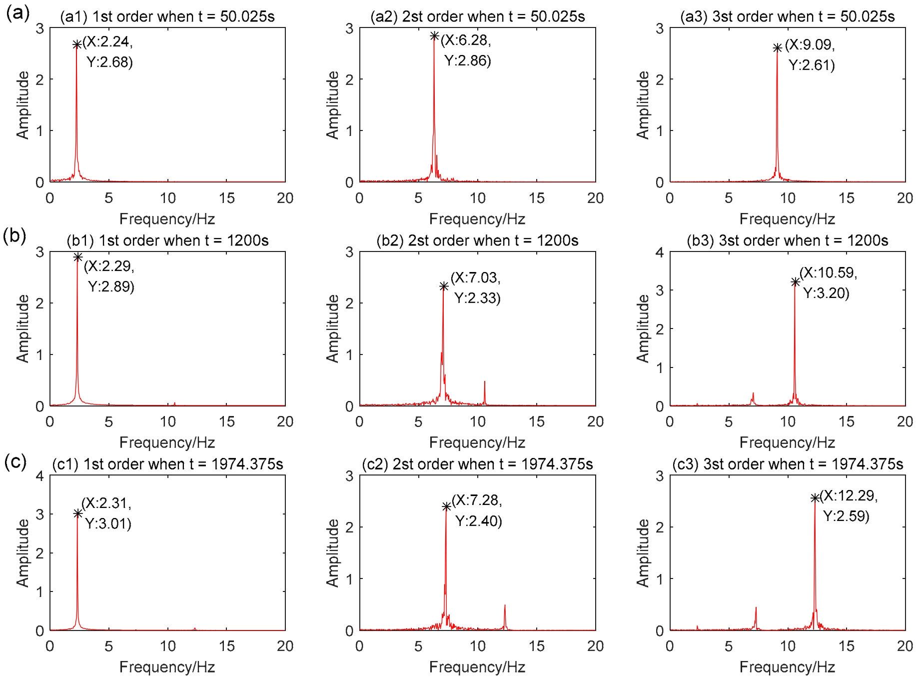

Figure 8. The natural frequency identified by MWLPP of the mass slow-time-varying 3-DOF structure when (**a**) t = 50.025 s, (**b**) t = 1200 s and (**c**) t = 1974.375 s.

4.1.2. A Density Slow-Time-Varying Cantilever Beam Structure

The density slow-time-varying cantilever beam structure is more complicated, as shown in Figure 9. One end of the cantilever beam is a fixed support, the other end is a free end, and many actual engineering structure can be simplified as a cantilever beam. Therefore, the modal parameters identified in the cantilever beam data set are also valuable.

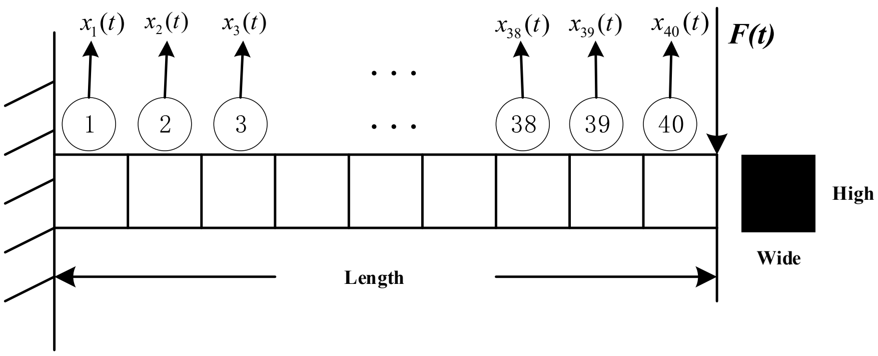

Figure 9. The density slow-time-varying cantilever beam structure with external force.

Assuming that the shear deformation of the cantilever beam is ignored, the cantilever beam structure is evenly divided into 40 elements using the finite element method. At the same time, the axial displacement of the beam is not considered, but only the vertical displacement and rotation angle.

Parameter Settings: the beam is 1 m in length, 0.02 m in width, 0.02 m in height and $Area = \text{width} \times \text{height} = 4 \times 10^{-4}\,\text{m}^2$ in cross-sectional area, second moment of area is $I = [\text{width} \times (\text{height})^3]/12 = 1.3 \times 10^{-8}\,\text{m}^4$, tensile modulus is $E = 2.1 \times 10^{11}\,\text{N/m}^2$, Poisson ratio is $u = 0.3$, the density is $\rho_0 = 78.60\,\text{kg/m}^3$, $F(t)$ is the Gaussian white noise excitation applied to the cantilever beam structure.

In the finite element model of cantilever beam, the cantilever beam is divided into 40 units and the its equation of motion such as Equation (1) is established. In addition, mass matrix $\mathbf{M}^e$, damping matrix $\mathbf{C}^e$ and stiffness matrix $\mathbf{K}^e$ of each window can be expressed as:

$$\mathbf{M}^e = \rho_0 \times Area \times \mathbf{M}_c^e = \frac{\rho_0 \times L \times Area}{420}\begin{bmatrix} 156 & 22L & 54 & -13L \\ 22L & 4L^2 & 13L^2 & -3L^2 \\ 54 & 13L & 156 & -22L \\ -13L & -3L^2 & -22L & 4L^2 \end{bmatrix} \tag{18}$$

$$\mathbf{K}^e = EIK_c^e = \frac{EI}{L^3}\begin{bmatrix} 12 & 6L & -12 & 6L \\ 6L & 4L^2 & -6L & 2L^2 \\ -12L & -6L & 12 & -6L \\ 6L & 2L^2 & -6L & 4L^2 \end{bmatrix} \tag{19}$$

$$\mathbf{C}^e = \beta_M \mathbf{M}^e + \beta_K \mathbf{K}^e \tag{20}$$

where L represents window length, β_M and β_K are proportional coefficients. Then the mass matrix $\mathbf{M}^e$, damping matrix $\mathbf{C}^e$ and stiffness matrix $\mathbf{K}^e$ are assembled into the total mass matrix $\mathbf{MM}$, damping matrix $\mathbf{CC}$ and stiffness matrix $\mathbf{KK}$ of the system:

$$\begin{cases} \mathbf{MM} = \sum_e \mathbf{M}^e \\ \mathbf{CC} = \sum_e \mathbf{C}^e \\ \mathbf{KK} = \sum_e \mathbf{K}^e \end{cases} \tag{21}$$

Therefore, the modal parameter can be calculated by finite element method, and the mode frequency, mode shape and modal damping ratio can be expressed as:

$$f_r = \sqrt{\frac{\mathbf{KK}_r}{\mathbf{MM}_r}},\ r = 1, 2, \cdots, N \tag{22}$$

$$(\mathbf{KK}_r - f_r^2 \mathbf{MM}_r)\vec{\phi}_r = 0,\ r = 1, 2, \cdots, N \tag{23}$$

$$\xi_r = \frac{\mathbf{CC}_r}{2\sqrt{\mathbf{MM}_r \mathbf{KK}_r}},\ r = 1, 2, \cdots, N \tag{24}$$

where $\mathbf{MM}_r$, and $\mathbf{CC}_r$ are the r-th order of modal mass matrix, modal stiffness matrix and modal damping matrix respectively. f_r, $\vec{\phi}_r$ and ξ_r are the r-th order of natural frequency, modal shape, and damping ratio. N is the number of sensor.

To achieve the slow-time-varying condition, the density of the cantilever beam is changed with time, as shown in Equation (25).

$$\rho_2 = \begin{cases} \rho_0,\ 0 \le t \le 0.5\,\mathrm{s} \\ \rho_0\,[1 - 0.08(t - 0.5)],\ 0.5\,\mathrm{s} < t \le 4\,\mathrm{s} \end{cases} \tag{25}$$

where rate of density change is 0.08, the total time is 4 s. Because the beam structure is a continuum rather than a multi-degree of freedom system, there are theoretically infinite modes. Even after discretization of a 40 degrees of freedom structure, there are theoretically 40 modes, the value of 700 Hz would not be sufficient then. In addition, the modal of the structure is generally concerned with the low frequency, and the analysis is only within 2000 Hz at most. Moreover, high-frequency noise is not considered in this article, so the sampling frequency of the structure is set at 10,000 Hz. The initial condition of the system is 0, and the density of the cantilever beam system remains unchanged in the first 0.5 s, in order to prevent the vibration system from being affected by random excitation in the initial stage of vibration. We took the data after 0.5 s for the simulation After 0.5 s, white noise excitation acts on the free end of the cantilever beam, and $Newmark - \beta$ method is adopted to collect the vibration response signal of displacement of each node on the beam. The time step of $Newmark - \beta$ method is $1/10,000$s, the parameter of β is 0.5, and the parameter of γ is 0.25, and the damping coefficient is $\beta_M = 4 \times 10^{-4}$, $\beta_K = 1 \times 10^{-7}$. The numerical simulation and algorithm writing of this paper are completed by using Matlab language and software. Finally, the displacement response $\mathbf{X}(t) \in \mathbb{R}^{40 \times 40,000}$ is obtained, and the 1st, 20th and 40th elements are plot in Figure 10. As long as the stability of the algorithm is guaranteed, the parameters could be set according to the requirements, unless the algorithm is very sensitive to noise numerically and generates bias. Of course, the higher sampling frequency, the $Newmark - \beta$ method for solving the vibration response signal of simulation data set are more accurate, the effect of modal identification are more accurate.

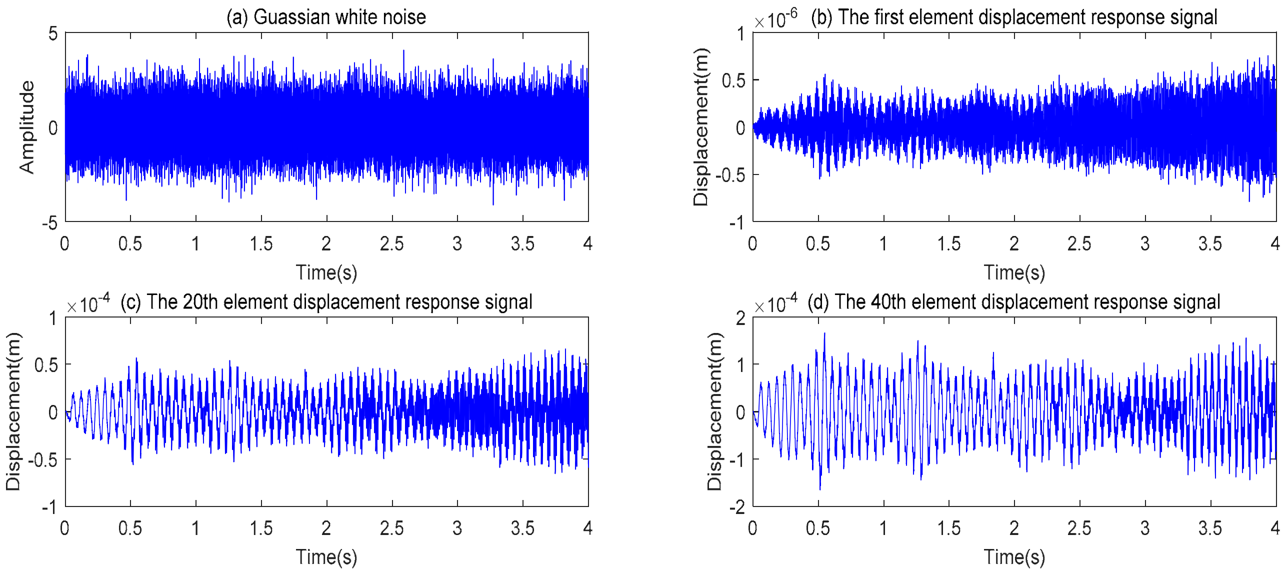

Figure 10. The Gaussian white noise (**a**) and 1st (**b**), 20th (**c**) and 40th (**d**) elements displacement response signal.

The real natural frequency variation of the first three modes of the structure is shown in Figure 11. The real natural frequencies of t = 0.5 s, t = 2 s and t = 3.795 s are shown in Table 2.

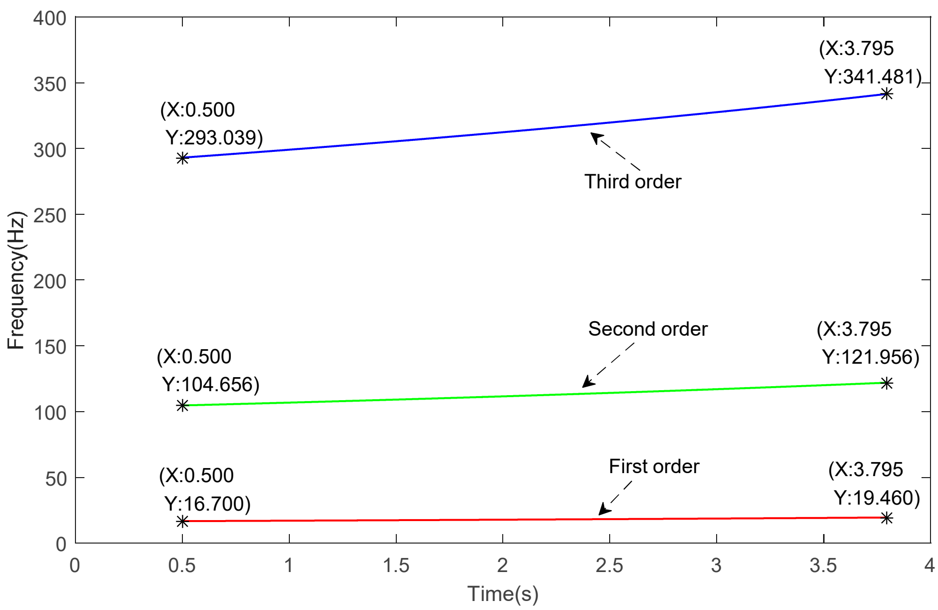

Figure 11. The real natural frequency of the density slow-time-varying cantilever beam structure.

Table 2. The real natural frequency of the density slow-time-varying cantilever beam structure when t = 0.5 s, t = 2 s and t = 3.795 s.

	Real Natural Frequency (Hz)		
Order	**t = 0.5 s**	**t = 2 s**	**t = 3.795 s**
1	16.70	17.80	19.46
2	104.66	111.56	121.96
3	293.03	312.38	341.48

4.2. The Evaluation Indexes

In the simulation, the average model assurance criterion (MAC_{i-avg}) will be used to identify the average accuracy of modal shapes. The specific definition of MAC_{i-avg} is,

$$\mathrm{MAC}_{i-avg} = \frac{1}{m}\sum_{j}^{m}\frac{(\vec{\phi}_{ij}{}^{T}\vec{\psi}_{ij})^{2}}{(\vec{\phi}_{ij}{}^{T}\vec{\phi}_{ij})(\vec{\psi}_{ij}{}^{T}\vec{\psi}_{ij})} \tag{26}$$

where $\vec{\phi}_{ij}$ is the modal shape of j-th window of the i-th order identified by algorithm; $\vec{\psi}_{ij}$ is real modal shape of j-th window of the i-th order identified; m is the number of windows. It can be seen from Equation (26) that the value range of MAC_{i-avg} is $0 \le \mathrm{MAC}_{i-avg} \le 1$. The closer the MAC_{i-avg} value is to 1, the higher the average identification accuracy of the modal shape of i-th order.

Average error rate (δ_{i-avg}) will be used to evaluate the natural frequency identified by algorithm. The specific definition of δ_{i-avg} is,

$$\delta_{i-avg} = \frac{1}{m}\sum_{j}^{m}\left|\frac{f_{ij} - f_{ij-real}}{f_{ij-real}}\right| \times 100\% \tag{27}$$

where f_{ij} is the natural frequency of j-th window of the i-th order identified by algorithm; $f_{ij-real}$ is real natural frequency of j-th window of the i-th order; m is the number of windows. It can be seen from Equation (27) that the value range of δ_{i-avg} is $\delta_{i-avg} \ge 0$. The closer the δ_{i-avg} value is to 0, the higher the average identification accuracy of the natural frequency of i-th order.

It is important to choose an appropriate limited memory length L of moving window. Frequency resolution $\triangle f$ and average frequency variation of the i-th modal in a window $\triangle f_L(i)$ was used to select window length. Window length L is proportional to sample frequency f_s and frequency resolution $\triangle f$, $\triangle f$ cannot be too small, because it cannot reflect the change of frequency, and $\triangle f$ cannot be too large, because the change of $\triangle f_L(i)$ cannot be identified, at the same time, $\triangle f_L(i)$ cannot be larger too much than $\triangle f$, otherwise, LTV structure cannot be regarded a LTI structure in a window. Therefore, different structures may choose different window lengths. The idea was proposed in [28,30].

$$\triangle f = \frac{f_s}{L} \tag{28}$$

$$\triangle f_L(i) = \frac{L}{f_s} \times \frac{f_{end}(i) - f_{begin}(i)}{t_{end} - t_{begin}} \tag{29}$$

where variables f_s, $f_{end}(i)$, $f_{begin}(i)$, t_{end}, t_{begin} are sample frequency, end-frequency of the i-th modal, begin-frequency of the i-th modal, end-time, begin-time of the whole data.

The model assurance criterion (MAC) will be used to identify the accuracy of modal shapes. The specific definition of MAC is,

$$\mathrm{MAC} = \frac{(\vec{\phi}^T \vec{\psi})^2}{(\vec{\phi}^T \vec{\phi})(\vec{\psi}^T \vec{\psi})} \tag{30}$$

where $\vec{\phi}$ is the modal shape identified by algorithm; $\vec{\psi}$ is real modal shape. The value range of MAC is $0 \leq \mathrm{MAC} \leq 1$. The closer the MAC value is to 1, the higher the identification accuracy of the modal shape.

4.3. The Parameter Settings

In the 3-DOF structure, the window length L is 1024, sample frequency f_s is 40 Hz and sample time is 2000 s. Frequency resolution is $\triangle f = 0.039$ Hz, the first average frequency variation is $\triangle f_L(1) = 9.25 \times 10^{-4}$Hz, the second average frequency variation is $\triangle f_L(2) = 0.0130$ Hz, the third average frequency variation is $\triangle f_L(3) = 0.0426$ Hz. Therefore, the length L = 1024 satisfies average frequency variation $\triangle f_L(i)$ cannot be lager too much than frequency resolution $\triangle f$.

In the cantilever beam structure, the window length L is 2048, sample frequency f_s is 10,000 Hz and sample time is 4 s. Frequency resolution is $\triangle f = 4.88$ Hz, the first average frequency variation is $\triangle f_L(1) = 0.15$ Hz, the second average frequency variation is $\triangle f_L(2) = 1.09$ Hz, the third average frequency variation is $\triangle f_L(3) = 3.06$ Hz. Therefore, the length L = 2048 satisfies average frequency variation $\triangle f_L(i)$ cannot be lager too much than frequency resolution $\triangle f$. The parameter K in LPP algorithm is 40, and the low-dimensional embedded dimension is 3.

4.4. Results

4.4.1. A mass Slow-Time-Varying 3-DOF Structure

In the linear slow-time-varying structure, the operational modal parameters of the system change at any time. The modal shapes at all times are difficult to describe. Therefore, in the mass slow-time-varying 3-DOF structure, we select four moments including t = 100 s, t = 650 s, t = 1500 s and t = 1974.375 s. Table 3 shows the MAC value at the instantaneous moment. Figure 12 shows the modal shape of the instantaneous moment. Figure 13 shows the time-varying natural frequencies identified by the MWLPP. Figure 14 shows the time-varying MAC values of modal shapes identified by the MWLPP. Table 4 shows the average error δ_{i-avg} of MWLPP and MWPCA in identifying natural frequencies. Figure 15 shows the change with time of damping ratio of slow-time-varying 3-DOF structure identified by MWLPP. In the identification process of operational modal parameters of structures, modal parameters of some windows (moments) are not identified, i.e., modal parameters are missing. Those windows that modal parameters are not identified are described as un-identified windows. Table 5 shows the number of un-identified windows between MWLPP and MWPCA. Table 6 shows the MAC_{i-avg} of modal shapes identified by MWLPP and MWPCA.

Table 3. The MAC (model assurance criterion) value of four moments including t = 100 s, t = 650 s, t = 1500 s and t = 1974.375 s in the mass slow-time-varying 3-DOF structure.

Order	t = 100 s	t = 650 s	t = 1500 s	t = 1974.375 s
1	1	1	0.9908	1
2	0.9999	0.9988	0.9746	0.7391
3	0.9998	1	0.9908	0.8691

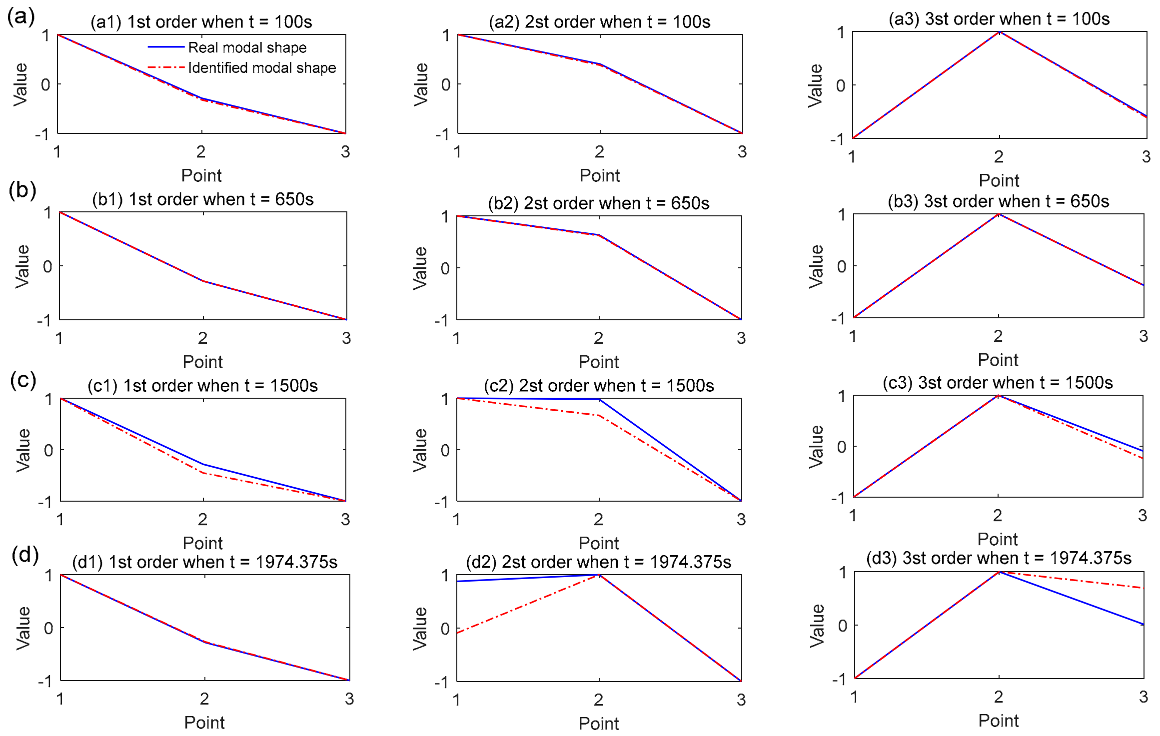

Figure 12. The modal shapes identified by MWLPP of four moments including (**a**) t = 100 s, (**b**) t = 650 s, (**c**) t = 1500 s and (**d**) t = 1974.375s in the mass slow-time-varying 3-DOF structure.

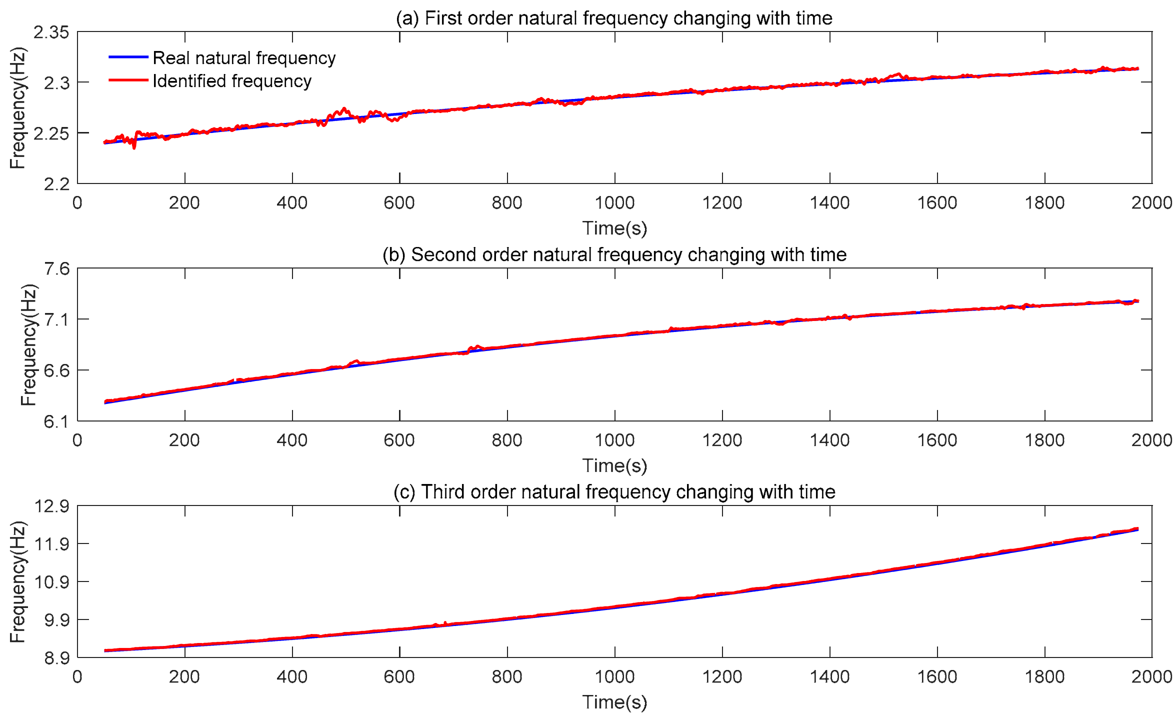

Figure 13. The natural frequencies identified by the MWLPP in the mass slow-time-varying 3-DOF structure.

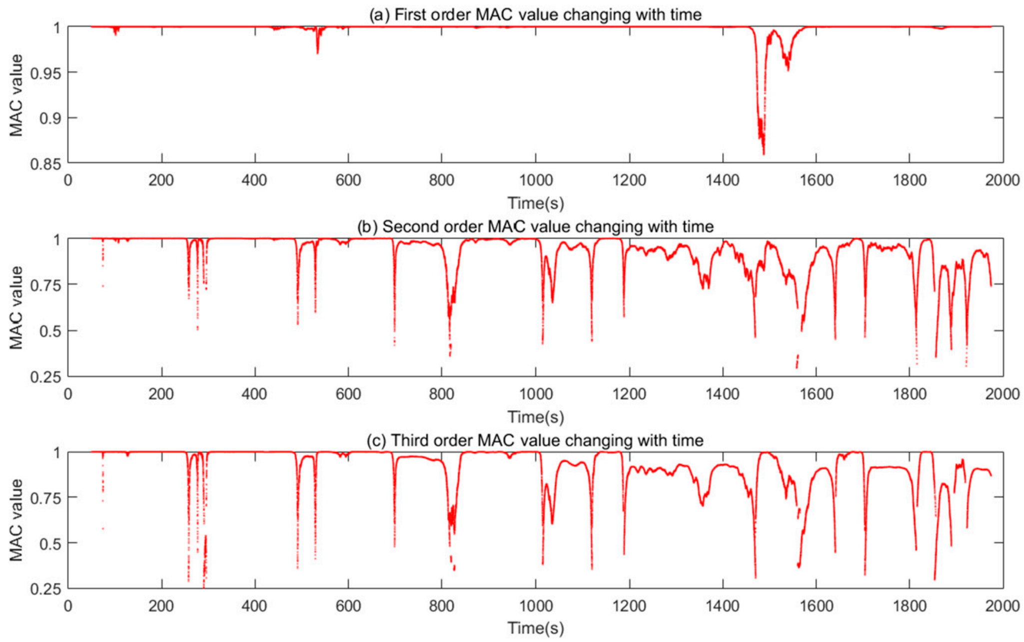

Figure 14. The MAC value of modal shapes identified by the MWLPP in the mass slow-time-varying 3-DOF structure.

Table 4. The average error δ_{i-avg} of MWLPP and MWPCA (moving window principal component analysis) in identifying natural frequencies in the mass slow-time-varying 3-DOF structure.

Method	Average Error δ_{1-avg}	Average Error δ_{2-avg}	Average Error δ_{3-avg}
MWLPP	0.059%	0.128%	0.244%
MWPCA	0.059%	0.129%	2.45%

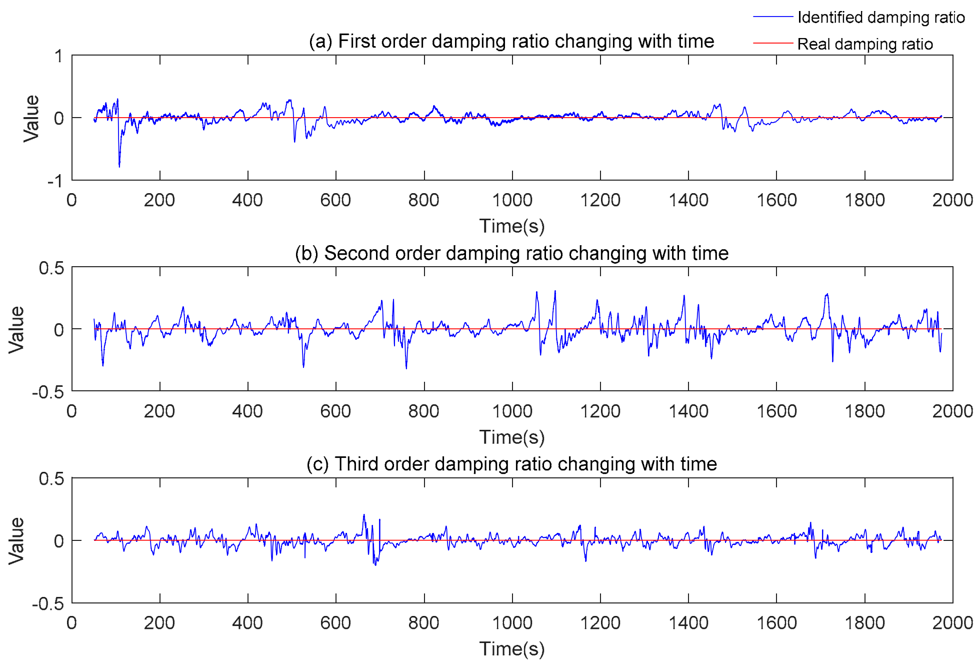

Figure 15. The change with time of damping ratio of slow-time-varying 3-DOF structure identified by MWLPP.

Table 5. The number of un-identified windows between MWLPP and MWPCA in the mass slow-time-varying 3-DOF structure.

Method	First Order Un-Identified Number	Rate	Second Order Un-Identified Number	Rate	Third Order Un-Identified Number	Rate
MWLPP	0	0	808	1.049%	747	0.970%
MWPCA	0	0	746	0.969%	1827	2.373%

Table 6. The MAC_{i-avg} of modal shapes identified by MWLPP and MWPCA in the mass slow-time-varying 3-DOF structure.

Method	MAC_{1-avg}	MAC_{2-avg}	MAC_{3-avg}
MWLPP	0.9979	0.9344	0.9254
MWPCA	0.9982	0.9009	0.9052

4.4.2. A Density Slow-Time-Varying Cantilever Beam Structure

In the density slow-time-varying cantilever beam structure, we select four moments including t = 0.75 s, t = 1.75 s, t = 2.75 s and t = 3.75 s. Table 7 shows the MAC value at the instantaneous moment. Figure 16 shows the modal shapes of the instantaneous moment. Figure 17 shows the time-varying natural frequencies identified by the MWLPP. Figure 18 shows the time-varying MAC values of modal shapes identified by the MWLPP. Table 8 shows the average error δ_{i-avg} of MWLPP and MWPCA in identifying natural frequencies. Table 9 shows the number of un-identified windows between MWLPP and MWPCA. Table 10 shows the MAC_{i-avg} of modal shapes identified by MWLPP and MW-PCA.

Table 7. The MAC value at four moments t = 0.75 s, t = 1.75 s, t = 2.75 s and t = 3.75 s of the density slow-time-varying cantilever beam structure.

Order	t = 0.75 s	t = 1.75 s	t = 2.75 s	t = 3.75 s
1	1	0.9998	0.9999	0.9997
2	0.9981	0.9858	0.9990	0.9988
3	0.9951	0.9742	0.9975	0.9947

Table 8. The average error δ_{i-avg} of MWLPP and MWPCA in identifying natural frequencies in the density slow-time-varying cantilever beam structure.

Method	Average Error δ_{1-avg}	Average Error δ_{2-avg}	Average Error δ_{3-avg}
MWLPP	3.234%	0.469%	0.159%
MWPCA	3.07%	0.470%	0.161%

Table 9. The number of un-identified windows between MWLPP and MWPCA in density slow-time-varying cantilever beam structure.

Method	First Order Un-Identified Number	Rate	Second Order Un-Identified Number	Rate	Third Order Un-Identified Number	Rate
MWLPP	0	0	6	0.018%	124	0.376%
MWPCA	213	0.64%	1	0.003%	66	0.2%

Table 10. The MAC_{i-avg} of modal shapes identified by MWLPP and MWPCA in the density slow-time-varying cantilever beam structure.

Method	MAC_{1-avg}	MAC_{2-avg}	MAC_{3-avg}
MWLPP	0.9990	0.9971	0.9789
MWPCA	0.9834	0.9773	0.8996

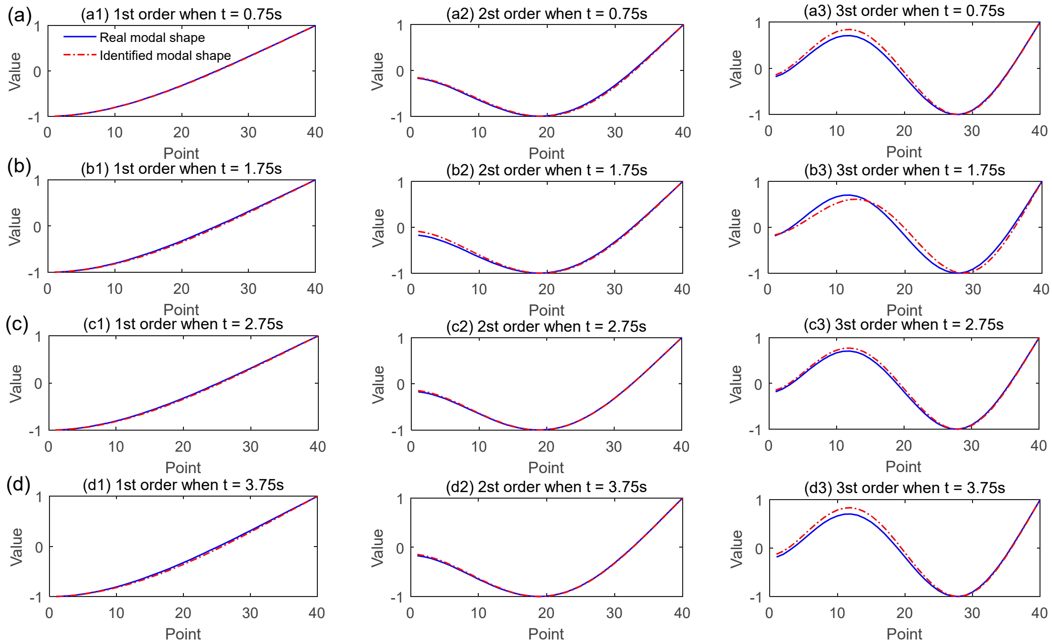

Figure 16. The modal shapes identified by MWLPP at four moments including (**a**) t = 0.75 s, (**b**) t = 1.75 s, (**c**) t = 2.75 s and (**d**) t = 3.75 s of the density slow-time-varying cantilever beam structure.

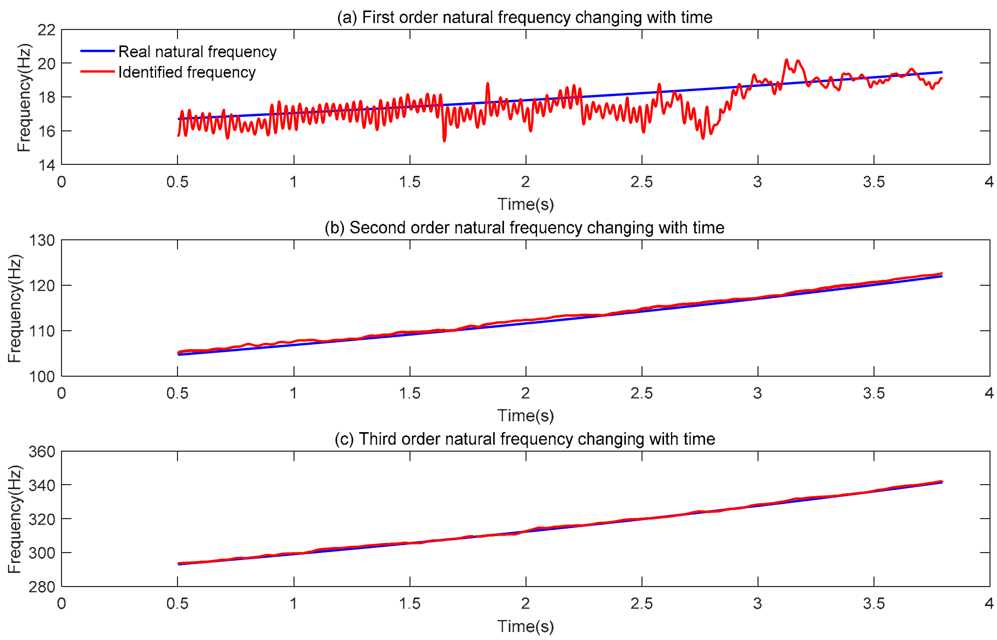

Figure 17. The natural frequencies identified by the MWLPP in the density slow-time-varying cantilever beam structure.

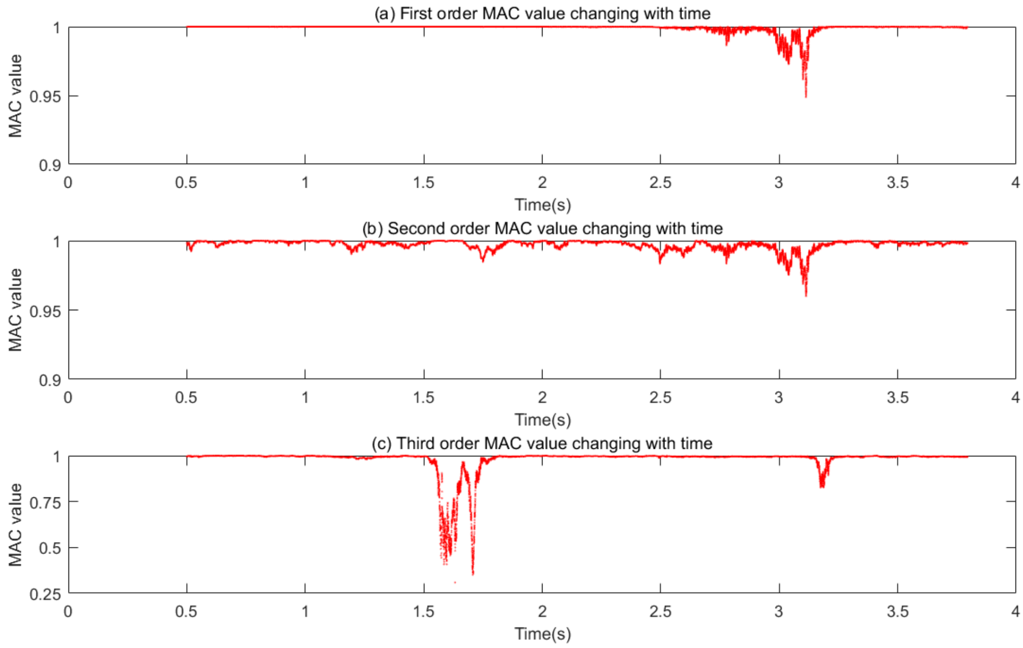

Figure 18. The MAC (model assurance criterion) value of modal shapes identified by the MWLPP in the density slow-time-varying cantilever beam structure.

4.4.3. A Mass Slow-Time-Varying 3-DOF Structure with 10% White Gaussian Noise

Ten percent white Gaussian noise is added to the vibration displacement response signal of the slow-time-varying 3-DOF structure, and the modal parameters of the structure are identified.

In the mass slow-time-varying 3-DOF structure with 10% white Gaussian noise, we also select four moments including t = 100 s, t = 650 s, t = 1500 s and t = 1974.375 s. Table 11 shows the MAC value at the instantaneous moment. Figure 19 shows the modal shape of the instantaneous moment. Figure 20 shows the time-varying natural frequencies identified by the MWLPP. Figure 21 shows the time-varying MAC values of modal shapes identified by the MWLPP. Table 12 shows the average error δ_{i-avg} of MWLPP in identifying natural frequencies. In the identification process of operational modal parameters of structures, modal parameters of some windows (moments) are not identified, i.e., modal parameters are missing. Those windows that modal parameters are not identified are described as un-identified windows. Table 13 shows the number of un-identified windows by MWLPP. Table 14 shows the MAC_{i-avg} of modal shapes identified by MWLPP.

Table 11. The MAC value of four moments including t = 100 s, t = 650 s, t = 1500 s and t = 1974.375 s in the mass slow-time-varying 3-DOF structure with 10% white Gaussian noise.

Order	t = 100 s	t = 650 s	t = 1500 s	t = 1974.375 s
1	0.9995	1	0.9938	1
2	0.9988	0.9997	0.9707	0.8243
3	0.9970	1	0.9818	0.8731

Table 12. The average error δ_{i-avg} of MWLPP in identifying natural frequencies in the mass slow-time-varying 3-DOF structure with 10% white Gaussian noise.

Method	Average Error δ_{1-avg}	Average Error δ_{2-avg}	Average Error δ_{3-avg}
MWLPP (with 10% white Gaussian noise)	0.059%	0.127%	0.245%
MWLPP (without white Gaussian noise)	0.059%	0.129%	2.45%

Table 13. The number of un-identified windows by MWLPP in the mass slow-time-varying 3-DOF structure with 10% white Gaussian noise.

Method	First Order Un-Identified Number	Rate	Second Order Un-Identified Number	Rate	Third Order Un-Identified Number	Rate
MWLPP (with 10% white Gaussian noise)	0	0	674	0.876%	1062	1.380%
MWLPP (without white Gaussian noise)	0	0	808	1.049%	747	0.970%

Table 14. The MAC_{i-avg} of modal shapes identified by MWLPP in the mass slow-time-varying 3-DOF structure with 10% white Gaussian noise.

Method	MAC_{1-avg}	MAC_{2-avg}	MAC_{3-avg}
MWLPP (with 10% white Gaussian noise)	0.9981	0.9260	0.9219
MWLPP (without white Gaussian noise)	0.9979	0.9344	0.9254

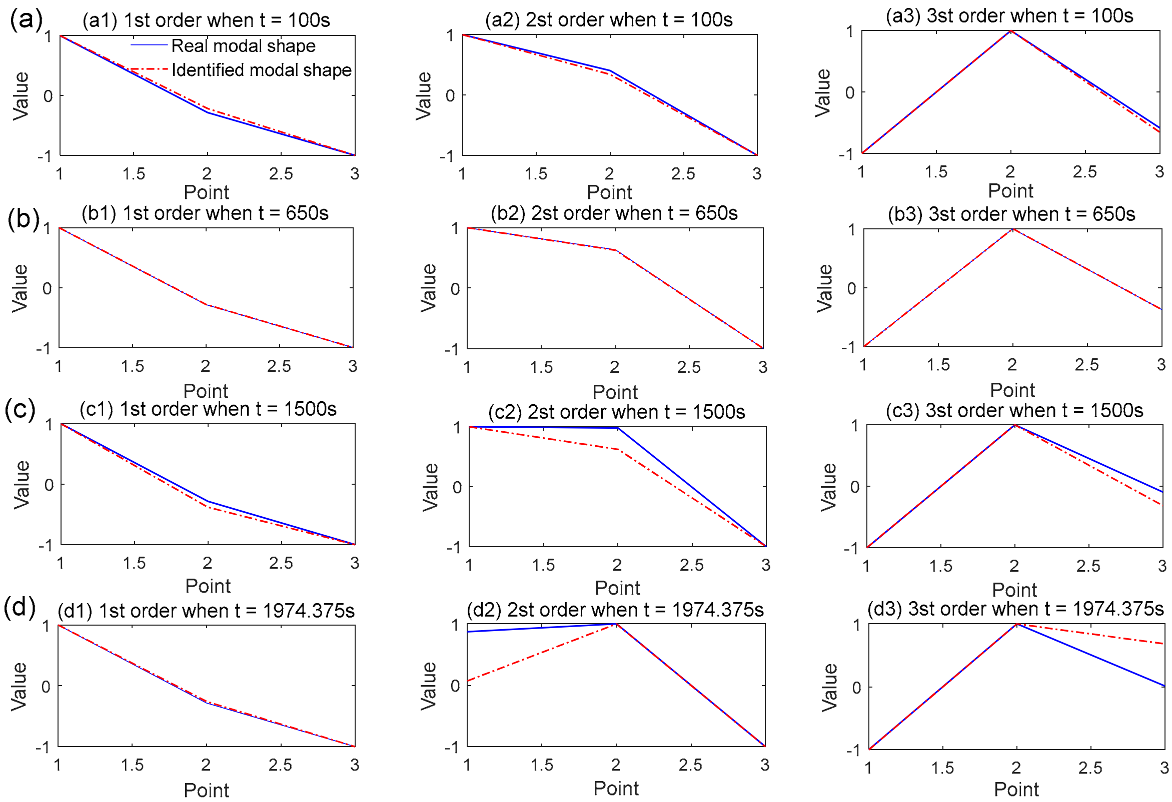

Figure 19. The modal shapes identified by MWLPP of four moments including (**a**) t = 100 s, (**b**) t = 650 s, (**c**) t = 1500 s and (**d**) t = 1974.375 s in the mass slow-time-varying 3-DOF structure with 10% white Gaussian noise.

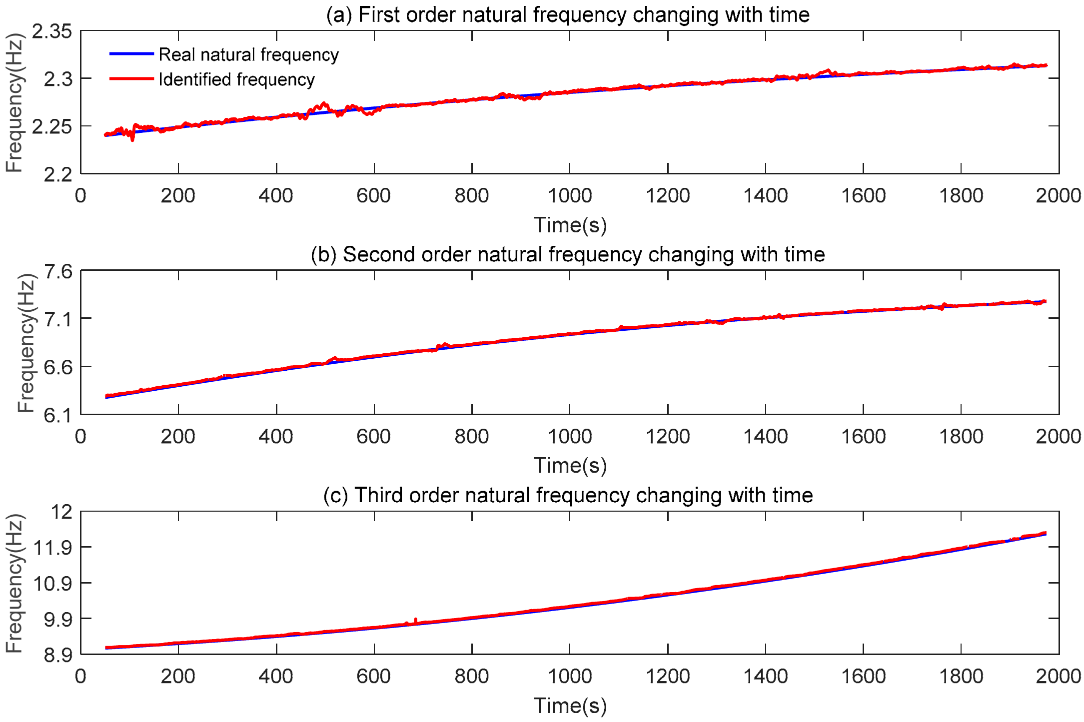

Figure 20. The natural frequencies identified by MWLPP in the mass slow-time-varying 3-DOF structure with 10% white Gaussian noise.

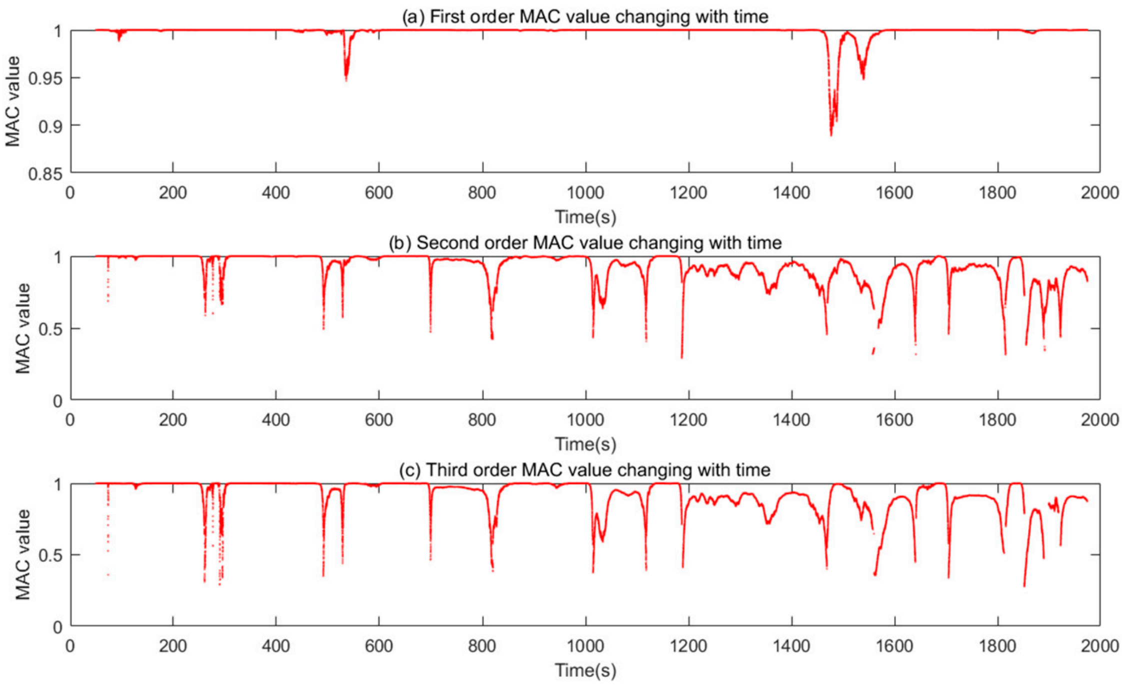

Figure 21. The MAC value of modal shapes identified by MWLPP in the mass slow-time-varying 3-DOF structure with 10% white Gaussian noise.

4.5. Analysis of Simulation Results

(1) From Figures 12–21 and Tables 3–14, the MWLPP method can identify the operational modal parameters of the slow time-varying structure well.

(2) Comparing Figures 12 and 16, and Tables 6 and 10, MWLPP has high accuracy in identifying modal shapes of linear slow-time-varying structures. In particular, MAC

values of modal shapes are very close to 1 in complex density slow-time-varying cantilever beam structures.

(3) Comparing Figures 13 and 17, the natural frequency of the linear slow-time-varying structure changing with time, and MWLPP can well track the change of the natural frequency. Combined with Tables 4 and 8, MWLPP has a high accuracy in identifying the natural frequency of the linear slow-time-varying structure.

(4) Comparing Tables 5 and 9, the total number of un-identified windows in MWLPP method is lower than that in MWPCA whether the structure is a linear mass slow-time-varying 3-DOF structure or a complex linear density slow-time-varying cantilever beam structure. Comparing Tables 6 and 10, the MAC value of modal shape identified by MWLPP is higher than that MWPCA. Therefore, the MWLPP method is superior to the MWPCA method in identifying the operational modal parameters of linear slow time-varying structures.

(5) From Figure 17 and Table 8, the first natural frequency seems contain fluctuations because the ordinate scale of the first mode natural frequency is small. According to Equation (29), in the cantilever beam structure, the first average frequency variation is $\triangle f_L(1) = 0.15$ Hz, the second average frequency variation is $\triangle f_L(2) = 1.09$ Hz, the third average frequency variation is $\triangle f_L(3) = 3.06$ Hz. The smaller the average frequency variation is, the smaller the variation range of the natural frequency value is. Due to the small variation range of the first order natural frequency value, the fluctuation phenomenon of the first order natural frequency is obvious in Figure 15 [28]. In addition, according to Equation (27), the denominator of the first order is much smaller than that of the second and the third order when calculating the average error rate δ_{i-avg} of natural frequency because the natural frequency value of the first order is smaller than that of the second and the third order. Therefore, in Table 8, the average error rate of natural frequency calculated in the first order is greater than that in the second and third order. In fact, the result of modal shape identification shows that the first order identification is indeed the best.

(6) Figure 15 shows that the damping ratio identified by MWLPP algorithm fluctuates greatly because theoretical analysis and numerical simulations indicate that a decreasing or moving mass and density will generate additional damping in the LTV structures [41,42]. In addition, compared with theoretical values, the identification accuracy of damping ratios has a certain error. It is generally predictable because the identification of the damping ratio itself is a difficult problem in the field of structural dynamics, and easily affected by the adopted identification algorithm. Therefore, the time-varying transient mode damping ratio identified by MWLPP is not suitable to compare with the mode damping ratio calculated by finite element methods.

(7) From Figures 14, 18 and 21, the MAC varies very much and have low values. The time-domain method used in this article cannot use the average technique in the frequency domain to identify the time-domain modes from the non-stationary random vibration response signals. Therefore, the algorithm is unstable, and some moments cannot identify the modal parameters, or the identified modal natural frequency and modal shape are not good. In addition, references [16,43] indicate that the change of damping will affect the performance of the algorithm in identifying modal parameters. From the Figure 15, damping ratio of time-varying structure constantly changing, which leads to low precision of modal parameter identification in some time. In addition, References [28,30] indicate that the window length L will also affect the identification accuracy of modal parameters. From Equation (28), the window length L is proportional to the sample frequency f_s and frequency resolution $\triangle f$. Frequency resolution $\triangle f$ cannot be too small, because it cannot reflect the change of frequency, and cannot be too large, because the average frequency variation $\triangle f_L(i)$ cannot be identified. At the same time, $\triangle f_L(i)$ cannot be larger too much than $\triangle f$, otherwise, time-varying structure cannot be regarded a time-invariant structure in a window.

(8) According to the noise simulation results of 3-DOF structure, the MWLPP algorithm turns out to be robust to noise. This is probably LPP algorithm computes a transformation matrix which maps the data points to a subspace. This linear transformation optimally preserves local neighborhood information in a certain sense [36]. This feature helps retain information about the response signal.

5. Conclusions

In this paper, a new method based on MWLPP for identifying operational modal parameters of linear slow-time-varying structures is presented. The low-dimensional embedding calculated by LPP algorithm corresponds to the modal coordinate response matrix, the transformation matrix corresponds to the modal shape matrix, and the operational modal parameters of the linear slow-time-varying structure are identified by the moving window method. Compared with the moving window principal component analysis method, MWLPP has higher accuracy and less modal missing in identifying the operational modal parameters of linear slow-time-varying structures.

However, fixed window length is an important parameter. How to determine and change the fixed length of moving window adaptively by non-stationary vibration response signal has not been solved completely. It is of great significance to apply this method to practical engineering structures. In addition, a further study is to establish a practical experiment to verify the effectiveness of the method.

Author Contributions: Conceptualization, W.F. and C.W.; methodology, W.F.; software, W.F.; validation, W.F.; formal analysis, W.F.; investigation, W.F.; resources, C.W. and J.C.; data curation, C.W.; writing—original draft preparation, W.F.; writing—review and editing, W.F. and C.W.; visualization, W.F.; supervision, C.W. and J.C.; project administration, C.W.; funding acquisition, C.W. All authors have read and agreed to the published version of the manuscript.

Funding: This work was financially supported by National Natural Science Foundation of China (Grant No. 51305142,51305143), National Key Technology R&D Program of China (No.2018YFB1402500), the Social Science Planning Foundation of Fujian Province (FJ2020B0033) and the Scientific Research Funds of Huaqiao University (16BS304), the General Financial Grant from the China Postdoctoral Science Foundation(Grant No:2014M552429), project of Quanzhou science and technology plan (2018C110R, 2018C114R), the first batch of youth innovation fund projects in 2020 (3502Z20206012).

Institutional Review Board Statement: Not applicable.

Informed Consent Statement: Not applicable.

Data Availability Statement: Not applicable.

Conflicts of Interest: The authors declare that there is no conflict of interest regarding the publication of this paper and regarding the funding that they have received.

References

1. Huang, Z.; Li, Y.; Hua, X.; Chen, Z.; Wen, Q. Automatic Identification of Bridge Vortex-Induced Vibration Using Random Decrement Method. *Appl. Sci.* **2019**, *9*, 2049. [CrossRef]
2. Brandt, A.; Berard, M.; Manzoni, S.; Vanali, M.; Cigada, A. Global scaling of operational modal analysis modes with the OMAH method. *Mech. Syst. Signal Process.* **2019**, *117*, 52–64. [CrossRef]
3. Lee, J. Estimation Modal Parameter Variation with Respect to Internal Energy Variation Based on the Iwan Model. *Appl. Sci.* **2019**, *9*, 4290. [CrossRef]
4. Nagarajaiah, S.; Basu, B. Output only identification and structural damage detection using time frequency and wavelet techniques. *Earthq. Eng. Eng. Vib.* **2010**, *8*, 583–605. [CrossRef]
5. Nabuco, B.; Tarpø, M.; Tygesen, U.; Brincker, R.; Zhao, G. Fatigue Stress Estimation of an Offshore Jacket Structure Based on Operational Modal Analysis. *Shock Vib.* **2020**, *2020*, 7890247.
6. Neu, E.; Janser, F.; Khatibi, A.; Braun, C.; Orifici, A. Operational Modal Analysis of a wing excited by transonic flow. *Aerosp. Sci. Technol.* **2016**, *49*, 73–79. [CrossRef]
7. Aşıkoğlu, A.; Avşar, Ö.; Lourenço, P.B.; Silva, L.C. Effectiveness of seismic retrofitting of a historical masonry structure: Kütahya Kurşunlu Mosque, Turkey. *Bull. Earthq. Eng.* **2019**, *17*, 3365–3395. [CrossRef]

8. Tenenbaum, J.; De-Silva, V.; Langford, J. A global geometric framework for nonlinear dimensionality reduction. *Science* **2000**, *290*, 2319–2323. [CrossRef]
9. Jain, A.; Dubes, R. Algorithms for Clustering Data. *Technometrics* **1988**, *32*, 227–229.
10. Wold, S.; Esbensen, K.; Geladi, P. Principal Component Analysis. *Chemometr. Intell. Lab.* **1987**, *2*, 37–52. [CrossRef]
11. Mukund, B.; Schwartz, E. The Isomap Algorithm and Topological Stability. *Science* **2002**, *295*, 7a-7.
12. Belkin, M.; Niyogi, P. Laplacian Eigenmaps and Spectral Techniques for Embedding and Clustering. *Adv. Neural Inf. Process. Syst.* **2002**, *14*, 585–591.
13. Sam, T.; Lawrence, K. Nonlinear Dimensionality Reduction by Locally Linear Embedding. *Science* **2000**, *290*, 2323–2326.
14. Wang, C.; Gou, J.; Bai, J.; Yan, G. Modal parameter identification with principal component analysis. *J. Xi'an Jiaotong Univ.* **2013**, *47*, 97–104.
15. Bai, J.; Yan, G.; Wang, C. Modal Identification Method Following Locally Linear Embedding. *J. Xi'an Jiaotong Univ.* **2013**, *47*, 85–89+100.
16. Wang, C.; Fu, W.; Huang, H. Isomap-Based Three-Dimensional Operational Modal Analysis. *Sci. Program. Neth.* **2020**, *2020*, 1–18. [CrossRef]
17. Dong, X.; Man, J.; Wang, H.; Yu, S.; Zhao, Y. Structural vibration monitoring and operational modal analysis of offshore wind turbine structure. *Ocean Eng.* **2018**, *150*, 280–297. [CrossRef]
18. Verboven, P.; Cauberghe, B.; Guillaume, P.; Vanlanduit, S.; Parloo, E. Modal parameter estimation and monitoring for on-line flight flutter analysis. *Mech. Syst. Signal Process.* **2004**, *18*, 587–610. [CrossRef]
19. Bart, P.; Herman, V.; Frederik, V.; Patrick, G. Operational modal analysis for estimating the dynamic propertiesof a stadium structure during a football game. *Shock Vib.* **2007**, *14*, 283–303.
20. Poulimenos, A.G.; Fassois, S.D. Parametric time-domain methods for non-stationary random vibration modelling and analysis—A critical survey and comparison. *Mech. Syst. Signal Process.* **2006**, *20*, 763–816. [CrossRef]
21. Zhou, S.; Heylen, W.; Sas, P. Parametric modal identification of time-varying structures and the validation approach of modal parameters. *Mech. Syst. Signal Process.* **2014**, *47*, 94–119. [CrossRef]
22. Zhou, S.; Ma, Y.; Liu, L.; Kang, J.; Ma, Z.; Yu, L. Output-only modal parameter estimator of linear time-varying structural systems based on vector TAR model and least squares support vector machine. *Mech. Syst. Signal Process.* **2018**, *98*, 722–755. [CrossRef]
23. Yang, W. Study on Modal Parameter Estimation and On-Line Identification Technology for Linear Time-Varying Structures in Time-Domain. Ph.D. Thesis, Beijing Institute of Technology, Beijing, China, 2015.
24. Ramnath, R. *Multiple Scales Theory and Aerospace Applications*; AIAA: Reston, VA, USA, 2015.
25. Li, J.; Zhu, X.; Law, S.; Samali, B. Time-varying characteristics of bridges under the passage of vehicles using synchroextracting transform. *Mech. Syst. Signal Process.* **2020**, *140*, 106727. [CrossRef]
26. Kopmaz, O.; Anderson, K. On the Eigenfrequencies of a Flexible Arm Driven by a Flexible Shaft. *J. Sound Vib.* **2001**, *240*, 679–704. [CrossRef]
27. Huang, H.; Wang, C.; Li, H. Moving Window Variable Step-size EASI Based Operational Modal Parameter Identification for Slow Linear Time-varying Structure. *Comput. Integr. Manuf. Syst.* **2020**, *2020*, 1–18.
28. Wang, C.; Wang, J.; Zhang, T. Operational modal analysis for slow linear time-varying structures based on moving window second order blind identification. *Signal Process.* **2017**, *133*, 169–186. [CrossRef]
29. Guan, W.; Wang, C.; Wang, T.; Zhang, H. Operational modal analysis for linear time-varying continuous cantilever beam dynamic structure based on LMPCA. *Int. J. Appl. Electrom.* **2016**, *52*, 1–9.
30. Wang, C.; Guan, W.; Wang, J. Adaptive operational modal identification for slow linear time-varying structures based on frozen-in coefficient method and limited memory recursive principal component analysis. *Mech. Syst. Signal Process.* **2017**, *100*, 899–925. [CrossRef]
31. Wang, C.; Huang, H.; Lai, X.; Chen, J. A New Online Operational Modal Analysis Method for Vibration Control for Linear Time-Varying Structure. *Appl. Sci.* **2020**, *10*, 48. [CrossRef]
32. Du, X.; Wang, F. Modal identification based on Gaussian continuous time autoregressive moving average model. *J. Sound Vib.* **2010**, *329*, 4294–4312.
33. Vu, V.; Thomas, M.; Lakis, A.; Marcouiller, L. Operational modal analysis by updating autoregressive model. *Mech. Syst. Signal Process.* **2011**, *25*, 1028–1044. [CrossRef]
34. Barros, J.; Roux, R.; Lopez, Z.; Martinez, R. Frequency and damping identification in flutter flight testing using singular value decomposition and QR factorization. *Proc. Inst. Mech. Eng. Part G J. Aerosp. Eng.* **2015**, *229*, 323–332. [CrossRef]
35. Chen, Z.; Chan, T.; Nguyen, A.; Yu, L. Identification of vehicle axle loads from bridge responses using preconditioned least square QR-factorization algorithm. *Mech. Syst. Signal Process.* **2019**, *128*, 479–796. [CrossRef]
36. He, X. Locality preserving projections. *Adv. Neural Inf. Process. Syst.* **2003**, *16*, 186–197.
37. Yang, J.; Lei, Y.; Lin, S.; Huang, N. Identification of Natural Frequencies and Dampings of In Situ Tall Buildings Using Ambient Wind Vibration Data. *J. Eng. Mech.* **2004**, *130*, 570–577. [CrossRef]
38. Kerschen, G.; Poncelet, F.; Golinval, J. Physical interpretation of independent component analysis in structural dynamics. *Mech. Syst. Signal Process.* **2007**, *21*, 1561–1575. [CrossRef]
39. Poncelet, F.; Kerschen, G.; Golinval, J.; Verhelstet, D. Output-only modal analysis using blind source separation techniques. *Mech. Syst. Signal Process.* **2007**, *21*, 2335–2358. [CrossRef]

40. Klepka, A.; Uhl, T. Identification of modal parameters of non-stationary systems with the use of wavelet based adaptive filtering. *Mech. Syst. Signal Process.* **2014**, *47*, 21–34. [CrossRef]
41. Ma, C.; Zhang, X.; Luo, Y. Dynamic analysis on a fluid-structure coupling system with variable mass in a rectangular tank. *J. Xi'an Jiaotong Univ.* **2014**, *48*, 109–116.
42. Ma, C.; Zhang, X.; Luo, Y.; Zhang, S. Dynamic responses for a fluid-structure coupling system with variable mass in a tank of spacecraft. *J. Aerosp. Power* **2015**, *330*, 736–745.
43. Zhou, W.; Chelidze, D. Blind source separation based vibration mode identification. *Mech. Syst. Signal Process.* **2007**, *21*, 3072–3087. [CrossRef]